Sec66-Dependent Regulation of Yeast Spindle-Pole Body Duplication Through Pom152

Santharam S. Katta,* Jingjing Chen,* Jennifer M. Gardner,* Jennifer M. Friederichs,* Sarah E. Smith,* Madelaine Gogol,* Jay R. Unruh,* Brian D. Slaughter,* and Sue L. Jaspersen*,†,1

*Stowers Institute for Medical Research, Kansas City, Missouri 64110, and †Department of Molecular and Integrative Physiology, University of Kansas Medical Center, Kansas City, Kansas 66160

ABSTRACT In closed mitotic systems such as *Saccharomyces cerevisiae*, the nuclear envelope (NE) does not break down during mitosis, so microtubule-organizing centers such as the spindle-pole body (SPB) must be inserted into the NE to facilitate bipolar spindle formation and chromosome segregation. The mechanism of SPB insertion has been linked to NE insertion of nuclear pore complexes (NPCs) through a series of genetic and physical interactions between NPCs and SPB components. To identify new genes involved in SPB duplication and NE insertion, we carried out genome-wide screens for suppressors of deletion alleles of SPB components, including Mps3 and Mps2. In addition to the nucleoporins *POM152* and *POM34*, we found that elimination of *SEC66*/*SEC71*/*KAR7* suppressed lethality of cells lacking *MPS2* or *MPS3*. Sec66 is a nonessential subunit of the Sec63 complex that functions together with the Sec61 complex in import of proteins into the endoplasmic reticulum (ER). Cells lacking Sec66 have reduced levels of Pom152 protein but not Pom34 or Ndc1, a shared component of the NPC and SPB. The fact that Sec66 but not other subunits of the ER translocon bypass deletion mutants in SPB genes suggests a specific role for Sec66 in the control of Pom152 levels. Based on the observation that *sec66Δ* does not affect the distribution of Ndc1 on the NE or Ndc1 binding to the SPB, we propose that Sec66-mediated regulation of Pom152 plays an NPC-independent role in the control of SPB duplication.

KEYWORDS Mps3; Sec66/Sec71/Kar7; spindle-pole body; Pom152; Nbp1

ACCURATE transmission of genetic material to daughter cells during cell division requires two precise duplication events: DNA replication and centrosome duplication. In addition, the cell must increase the number of organelles and protein complexes such as ribosomes and nuclear pore complexes (NPCs) so that the daughter cells have material to continue cell growth, metabolism, transcription, translation, and other vital cellular processes. While much is known about the mechanism and regulation of DNA replication, less is known about how cells duplicate protein-based structures such as the centrosome once per cell cycle.

doi: 10.1534/genetics.115.178012
Manuscript received May 7, 2015; accepted for publication October 23, 2015; published Early Online October 26, 2015.
Available freely online through the author-supported open access option.
Supporting information is available online at www.genetics.org/lookup/suppl/doi:10.1534/genetics.115.178012/-/DC1
Data were submitted to the GEO database at NCBI as accession number GSE73681.
[1]Corresponding author: Stowers Institute for Medical Research, 1000 E. 50th St., Kansas City, MO 64110. E-mail: slj@stowers.org

The spindle-pole body (SPB) is the *Saccharomyces cerevisiae* centrosome-equivalent organelle and is perhaps one of the best-characterized microtubule organizing centers (Jaspersen and Winey 2004; Kilmartin 2014). Cytologic studies of the SPB showed that it is embedded in the nuclear envelope (NE) throughout the yeast life cycle, where it nucleates cytoplasmic microtubules that are important for nuclear positioning and mating and spindle microtubules that are essential for chromosome segregation during mitosis and meiosis (Winey and Bloom 2012). Conventional electron microscopy (EM) and electron tomography revealed that the SPB is a multilayered structure that is attached to the NE via hooklike appendages (Byers and Goetsch 1974, 1975; O'Toole *et al.* 1999). One side of the SPB is associated with an electron-dense region of the NE known as the *half-bridge*, which plays a key role in the control of SPB duplication and is likely involved in insertion of the SPB into the NE.

SPB duplication begins as cells exit mitosis by elongation of the half-bridge and deposition of the satellite (the SPB precursor) at its distal cytoplasmic tip (Byers and Goetsch 1975; Adams and Kilmartin 1999). During G_1, the satellite matures

into a structure known as the *duplication plaque*, and the extended bridge fuses at its tip, retracts, and bends underneath the duplication plaque. Finally, the duplication plaque is inserted into the NE, at which time nuclear SPB components can assemble to result in duplicated side-by-side SPBs.

A combination of molecular, biochemical, and genetic approaches led to the identification of 18 core components of the SPB, and all have been assigned a position within the SPB structure based on immuno-EM localization and physical interaction studies (Jaspersen and Winey 2004; Kilmartin 2014). Of the 18 core components, all but one or two (*CNM67* and, in some strains, *SPC72*) are essential for growth. Analysis of conditional hypomorphic mutations or degron alleles has suggested an order and a function for each gene product in SPB duplication, microtubule nucleation, or other functions such as exit from mitosis. Most mutations in components of the half-bridge, such as the membrane proteins Mps3 and Kar1 and the soluble filamentous Sfi1 protein and its binding partner Cdc31 (centrin), have defects in the early steps of SPB duplication (Baum *et al.* 1986; Vallen *et al.* 1992, 1994; Spang *et al.* 1993, 1995; Biggins and Rose 1994; Jaspersen *et al.* 2002; Kilmartin 2003), while most mutations in membrane pore components (Mps2 and Ndc1) and their binding partners (Bbp1 and Nbp1, respectively) arrest at the late step of SPB duplication, with a mature duplication plaque that is unable to insert into the NE (Winey *et al.* 1993; Chial *et al.* 1998; Munoz-Centeno *et al.* 1999; Schramm *et al.* 2000; Araki *et al.* 2006). Recent super-resolution imaging of duplicating SPBs suggests that membrane insertion may be coupled with SPB assembly in wild-type cells (Burns *et al.* 2015). The localization of Ndc1 and/or Nbp1 to the new SPB appears to be involved in the final step of SPB duplication, consistent with genetic analyses (Winey *et al.* 1993; Chial *et al.* 1998; Munoz-Centeno *et al.* 1999; Schramm *et al.* 2000; Araki *et al.* 2006).

In yeast as in other eukaryotes, NPCs are present at multiple locations in the NE to facilitate movement of macromolecules into and out of the nucleus. Like SPBs, NPCs are composed of a relatively small number of molecules that are present in multiple copies (Strambio-De-Castillia *et al.* 2010; Aitchison and Rout 2012). NPC assembly in postmitotic cells or in organisms such as yeast that undergo a closed mitosis, in which the nuclear membrane does not break down, occurs by a *de novo* pathway in which NPCs are inserted into an intact NE (Hetzer and Wente 2009). Cytologic, genetic, and molecular studies have linked the mechanism of *de novo* NPC assembly with that of SPB membrane insertion. Membrane-associated proteins that bind, bend, or stabilize curved membranes, including reticulons and ALPS (for ArfGAP1 lipid packing sensor) domain–containing proteins, are involved in SPB duplication and NPC assembly (Dawson *et al.* 2009; Doucet *et al.* 2010; Drin and Antonny 2010; Kupke *et al.* 2011; Casey *et al.* 2012; Kim *et al.* 2014). In addition, *NDC1* encodes a conserved integral membrane protein that localizes to both SPBs and NPCs, and analysis of yeast cells lacking Ndc1 function shows defects in NE insertion of both complexes (Chial *et al.* 1998; West *et al.* 1998; Lau *et al.* 2006; Madrid *et al.* 2006; Onischenko *et al.* 2009). The observation that mutation or deletion of genes encoding membrane and membrane-associated components of the SPB can be suppressed by elimination of Ndc1 binding partners at the NPC such as Pom152 or Pom34 has led to the idea that the SPB and NPC may compete for Ndc1 or other NE insertion factors (Chial *et al.* 1998; Sezen *et al.* 2009; Witkin *et al.* 2010; Casey *et al.* 2012). Consistent with this idea, we recently demonstrated that the distribution of Ndc1 between the NPC and SPB was altered by deletion of *POM152* (Chen *et al.* 2014). However, other suppression mechanisms may exist, including a translational control pathway that is activated following *POM34* deletion and/or alteration in the properties of the NE that may facilitate insertion of large complexes such as the SPB (Sezen *et al.* 2009; Witkin *et al.* 2010; Friederichs *et al.* 2011).

Here we characterized cells lacking *MPS3* and *POM152* to determine whether elimination of the nucleoporin Pom152 is able to suppress all known functions of Mps3, including its essential role in SPB duplication in mitosis and meiosis and its nonessential functions in chromosome organization within the nucleus. We then used genome-wide screening to identify other bypass suppressors of *mps3Δ* as well as other deletions in membrane (*mps2Δ* and *nbp1Δ*) and half-bridge (*cdc31Δ*, *kar1Δ*, and *sfi1Δ*) components of the SPB to better understand interactions between the SPB and NPC and to discover new factors that regulate SPB duplication and NE insertion. Further characterization of one bypass suppressor, *sec66Δ*, suggests that post-transcriptional control of Pom152 affects SPB duplication in a manner that is distinct from its role in the NPC.

Materials and Methods

Yeast methods

Standard techniques were used for DNA and yeast manipulations. All strains are listed in Supporting Information, Table S4. With the exception of strains used for chromosome loss and for the suppressor screen, strains are derivatives of W303. The yeast deletion collection was purchased from Open Biosystems in 2004. Deletion and tagging of genes were done using PCR-based methods and verified by PCR (Longtine *et al.* 1998; Sheff and Thorn 2004).

pRS425-derived plasmids (2μ-*LEU2*) containing *POM152* (pSJ998) or *POM34* (pSJ1652) were created by PCR amplification of the ORF plus ~500 bp of upstream sequence and ~200 bp of downstream sequence from genomic DNA derived from W303. The ORF of *POM152* also was amplified and cloned together with the *GAL1/10* promoter into pRS305 to create pRS305-*GAL1-POM152* (pSJ1655).

SPB suppressor screen

The SPB suppressor screen was done using a modified version of the protocol for synthetic genetic analysis described by Tong and Boone (2006). A centromeric *URA3*-marked plasmid containing a SPB gene and its flanking sequence was

transformed into the SGA query strain, and then the genomic copy of the SPB gene was deleted with a *NATMX* cassette using PCR, creating *MAT*α *spbΔ*::*NATMX can1Δ*::*STE2pr-HIS3MX lyp1Δ ura3 his3 YFG1 pURA3-SPB*. Each was mated to the deletion collection (*MAT***a** *yfgΔ*::*KANMX LYP1 CAN1 his3 ura3 SPB*) using the Singer RoToR, and diploids were selected on YPD + G418 + clonNAT. Cells were pinned to 5-fluoro-orotic acid (5-FOA) twice to select for loss of the covering plasmid, *pURA3-SPB*. Diploids were sporulated for 3–4 weeks, and then haploids were selected twice on SD-His-Lys-Arg + thialysine + canavanine before pinning to SD/MSG-His-Lys-Arg + thialysine + canavanine + G418 + clonNAT. All plates were incubated at 23°. Each screen was done in triplicate, and genes that rescued growth in at least two of the three screens are shown in Figure 2C, Table S1, and Table S2.

Suppressors of *mps3Δ* were further verified by complementation of the suppression phenotype using clones from the 2μ tiling library, if available (Jones *et al.* 2008). In addition, deletions were recreated in the W303 strain background using PCR-based methods. Only *pom152Δ*, *pom34Δ*, and *sec66Δ* suppressed *mps3Δ* in both BY and W303 strains.

Chromosome 13

Deletions in a small region of chromosome *13* were identified in all but one of our screens (Table S2). Many have been previously isolated in suppressor screens for other essential genes using synthetic genetic array (SGA) methodology (Copic *et al.* 2012). We performed array-based comparative genomic hybridization using eight deletion strains from this region in our copy of the *MAT***a** deletion collection and the isogenic wild-type strain BY4741 to determine whether the deletion strains carried a linked mutation that was responsible for the suppression phenotype. Six of eight strains (*UFO1*, *AIM33*, *ALO1*, *YML083C*, *YML082W*, and *DUS1*) contained the correct deletion; in the remaining two, one had the adjacent gene removed (*GAL80* instead had a deletion of *YML082W*), and the other (*RPS1B*) contained no detectable deletion. All eight strains also have a deficiency in *YML050W/AIM32*, a gene of unknown function. Although present in the deletion collection, this ORF was never recovered as a hit. Direct knockout of genes in this region individually or with *AIM32* did not bypass any SPB deletions. We suspect that deletion of one of these genes allows cells to escape a growth condition used in high-throughput screening, and thus diploids or one of the individual knockouts lives.

Chromosome assays

The position of GFP telomere spots was determined as described previously (Hediger *et al.* 2002). Briefly, a Zeiss Axio Imager with a 100× Zeiss alpha Plan-Fluar objective (NA = 1.45) and a Hamamatsu ORCA-ER digital camera were used to capture 19-image stacks of 170-nm step size through nuclei of log-phase cells at room temperature. The spot-to-periphery distance and the nuclear diameter were determined in a single-Z-stack image where the spot was most concentrated using Axiovision 4.6.3 (Zeiss), except in cases where the spot fell into one of the top or bottom three focal planes. By dividing the spot-to-periphery distance by the diameter, each spot fell into one of three zones of equal surface (Figure 1A). Zone 1 has a width of $0.184 \times$ the nuclear radius r, zone 2 has a width of $0.184 \times r$ to $0.422 \times r$, and zone 3 has a width of $0.422 \times r$. Confidence values (P-values) for the χ^2 test were calculated for each data set between random and test distributions.

Sister-chromatid cohesion was assayed in logarithmically growing cells that were arrested with 10 μg/ml nocodazole for 3 hr. Cells were briefly fixed with 4% paraformaldehyde and stained with DAPI before cell counting. In addition, aliquots of cells were removed for flow cytometric analysis of DNA content to verify the mitotic arrest. Chromosome loss assays and flow cytometric analysis of DNA content were performed as described previously (Spencer *et al.* 1990; Jaspersen *et al.* 2002). Fractional statistics were analyzed via the binomial distribution (Bevington and Robinson 2003). In Figure 1E, variation between colony replicates was somewhat larger than allowed by the binomial distribution. In such cases, P-values also were generated via t-tests between three colony replicates of each sample: *mps3Δ 75–150* and *pom152Δ mps3Δ* had P-values below 0.001, while *pom152Δ* had a P-value below 0.02, all indicating statistical significance.

Quantitative imaging

Live-cell imaging data were acquired on a PerkinElmer Ultraview Confocal Microscope with a Yokagawa CSU-X1 Spinning Disk on an inverted Zeiss 200 base. Emission was collected onto a C9100-13 Hamamatsu EM-CCD using Velocity software (PerkinElmer). An α Plan-Apochromat 100× 1.46-NA oil-immersion objective was used. GFP and mCherry images were acquired with 488- and 561-nm excitation, respectively, using a 405/488/561/640 dichroic. Emission filters were a 415- to 475-nm/580- to 650-nm dual-band filter for mCherry and a 500- to 550-nm filter for GFP. mTurquoise2 and yellow fluorescent protein (YFP) were excited with 440 and 514 nm, respectively, via a 405/440/514/640 dichroic. Emission filters were a 456- to 484-nm filter for mTurqouise2 and a 525- to 575-nm filter for YFP. All spinning-disk data were acquired in alternating excitation mode. For Z-stacks, a slice size of 400 nm was used.

Acceptor-photobleaching fluorescence resonance energy transfer (FRET)

Using the PhotoKinesis accessory on the PerkinElmer Ultraview Spinning Disk Confocal Microscope, cells expressing mTurquoise2 (donor) and YFP (acceptor) were imaged at maximum speed for a total of 10 frames. YFP at the SPB was bleached following frame 5 using 15 iterations with 100% of the 514-nm line. YFP fluorescence was checked following acquisition to ensure complete bleaching. Controls indicated no significant crosstalk of YFP fluorescence into the mTurquoise2 channel. Analysis was performed using ImageJ software: the center of the SPB was determined via a two-dimensional (2D) Gaussian fit, and the total intensity over

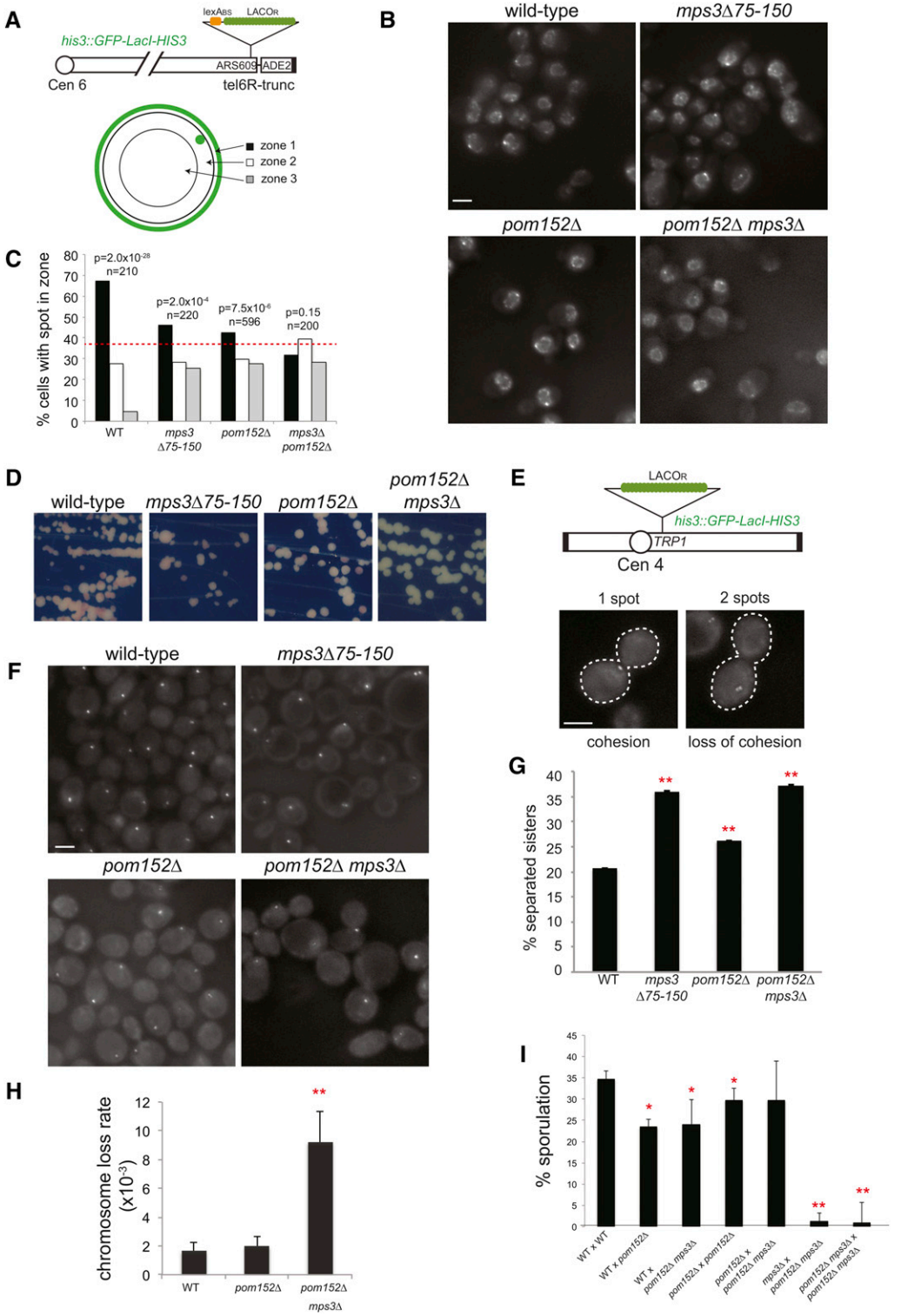

Figure 1 Deletion of *POM152* only bypasses the requirement for Mps3 at the SPB. (A) Schematic of chromosome *6* with ~256 copies of the $LacO_R$ and four $lexA^{op}$ binding sites integrated at ARS609, near a truncated version of telomere VI-R that contains the *ADE2* reporter linked to copies of the $TG_{1–3}$ telomeric repeats (Hediger *et al.* 2002). Expression of GFP-LacI and Nup49-GFP (a nucleoporin) in these cells allows the subnuclear position of the telomere to be scored with respect to the distance from the NE in a single-plane image and assigned a position in one of three zones of equal volume. (B) Single-plane images showing the localization of truncated telomere VI-R in wild-type (SLJ2602), *mps3Δ75–150* (SLJ3081), *pom152Δ* (SLJ4333), and *mps3Δ pom152Δ* (SLJ4330) cells. Note that in some cases the telomeric focus may be above or below the focal plane shown. The position of telomeres was scored in three dimensions. Bar, 5 μm. (C) Using bud morphology as a marker for cell cycle position, the location of telomeres in S-phase cells was determined. Zone 1, black bars; zone 2, white bars; and zone 3, gray bars. The red horizontal bar at 33% corresponds to a random distribution. Confidence intervals (*P*-values) for the χ^2 test were calculated for each data set between random and test distributions. The number of cells examined in each data set is indicated (*n*). (D) Expression of the telomeric *ADE2* gene in strains from B was assayed by streaking cells to SD plates containing 10 μg/ml adenine. Following growth for 3 days at 30°, plates were incubated for 1 week at 4° to allow the red pigment to develop. Expression of *ADE2* results in white-colored cells and blocks the accumulation of the red pigment in this strain background; this occurs in cells that have lost telomeric silencing. (E) Sister-chromatid cohesion was tested by arresting cells containing GFP-LacI and an ~256-bp $LacO_R$ array on the arm of chromosome *4* in mitosis using nocodazole. Under these conditions, a single GFP focus is indicative of cohesion, while the appearance of two foci indicates that cohesion has been lost. The cell outline is based on the DIC image. Bar, 5 μm. (F) Maximum-intensity projections of wild-type (SLJ1982), *mps3Δ75–150* (SLJ3131), *pom152Δ* (SLJ4328), and *mps3Δ pom152Δ* (SLJ4325) cells. Bar, 5 μm. (G) The percentage of large-budded cells from F that contained two distinct GFP foci was determined in two independent experiments using three biological replicates. Average values from the six samples are shown; error bars show the 95% confidence interval based on the binomial test, and error bars show the SD from the mean. $^{**}P < 0.0001$. Statistical analysis of individual isolates using the *t*-test also showed significance between samples at $P = 0.02$ or greater. (H) Loss of an artificial chromosome *3* fragment containing *SUP11* was assayed in wild-type (SLJ2156), *pom152Δ* (SLJ4547), and *mps3Δ pom152Δ* (SLJ4548) cells. The average loss rate from three independent experiments is shown along with the SEM. $^{**}P < 0.0001$. (I) Diploid strains of the indicated genotypes were grown overnight at 23° in YPA before being transferred to sporulation medium for 5 days at 23°. Meiotic progression was analyzed based on DAPI staining and DIC images. The percentage of unsporulated cells and sporulated cells that formed dyads (two DNA masses in two spores per ascus) or tetrads (four DNA masses in four spores per ascus) was determined ($n = 200$) in three independent experiments (error bars, SEM; $^{*}P < 0.01$; $^{**}P < 0.0001$).

time was calculated for of a 9 × 9 square centered at the initial position of the SPB. The background-subtracted values for the pre- and postbleach time series then were each fit to a linear regression, and the value of each at time point 5.5 was interpolated. FRET was then calculated from the donor intensity as 100 × (postbleach − prebleach)/postbleach. To eliminate artifacts owing to SPB movement, the 2D Gaussian fit was calculated over time, and SPBs were removed from analysis if, in either pre- or postbleach time series, SPB centers moved more than 1 pixel in x or y or the SD of the Gaussian fit changed more than 0.5 pixel.

RNA-Seq analysis

Starting with total RNA from three replicates of wild-type and *sec66Δ* cells, polyA RNA was isolated and prepared for sequencing using a TruSeq RNA Sample Prep Kit (Illumina). Indexed samples were pooled and sequenced in a single-flow cell on an Illumina HiSeq. Five of six samples generated 10–11 million reads each, and one wild-type sample generated 5.6 million reads. Using TopHat 2.0.10, reads were aligned to the saCer3 genome from UCSC with gene annotations from Ensembl 72., and counts were normalized using edgeR. Differentially expressed genes listed in Table S3 showed a twofold increase (27) or decrease (91) in the mutant *vs.* wild-type cells [$P < 0.05$ and average $\log_2$(normalized counts) > 0]. SPB, NPC, and membrane encoding genes depicted in Figure 3E were identified based on annotations in the Saccharomyces Genome Database (SGD).

Western blotting

Whole-cell extracts were prepared by bead beating into SDS sample buffer. The following primary antibody dilutions were used: 1:1000 anti-GFP (Cell Signaling Technology) and 1:5000 anti-Pgk1 (Life Technologies). Alkaline phosphatase–conjugated secondary antibodies were used at 1:10000 (Promega), and fluorescently labeled secondaries were used at 1:5000 (LiCor).

Data availability

Original data underlying this manuscript can be downloaded from the Stowers Original Data Repository at http://www.stowers.org/pubs/LIBPB-1004.

Results

Characterization of cells lacking MPS3

The Mps3 C-terminus, which includes the conserved SUN domain, is essential for SPB duplication (Nishikawa *et al.* 2003; Jaspersen *et al.* 2002, 2006). Previously, we showed that the growth defect of C-terminal *MPS3* mutants could be rescued if *POM152* was eliminated from the genome. In addition, the lethality associated with deletion of *MPS3* is suppressed by removal of *POM152*, suggesting that the essential SPB function of Mps3 is bypassed (Witkin *et al.* 2010; Friederichs *et al.* 2011). At least two models could explain this suppression: first, *pom152Δ* might act as a "dosage suppressor" by freeing factors from the NPC that are involved in both NPC and SPB assembly, and second, reduced NPC assembly in *pom152Δ* may indirectly result in NE changes that allow SPB duplication in the absence of *MPS3* (Jaspersen and Ghosh 2012).

To better understand the mechanism of *pom152Δ*-based suppression, we analyzed the nonessential functions of Mps3 in *pom152Δ mps3Δ* cells. Although the Mps3 N-terminus is not required for mitotic growth, cells lacking amino acids 75–150 (*mps3Δ75–150*) display defects in chromosome organization, including loss of telomere tethering and silencing and defects in sister-chromatid cohesion following DNA replication (Antoniacci *et al.* 2004; Bupp *et al.* 2007; Schober *et al.* 2009; Ghosh *et al.* 2012). A different region of the Mps3 N-terminus (amino acids 2–64) is required for meiotic chromosome reorganization and movement (Conrad *et al.* 2007). We hypothesized that if *pom152Δ* suppresses the requirement for Mps3 by liberating a SPB insertion factor, it would likely suppress only the SPB function of Mps3, and *pom152Δ mps3Δ* cells would be defective in other Mps3-dependent processes, similar to *mps3Δ75–150* or *mps3Δ2–64* mutants. However, if suppression arises as a consequence of altered NE properties, then deletion of *POM152* may reduce or eliminate the need for Mps3 in its other functions, such as chromosome positioning during S phase, sister-chromatid cohesion, or meiotic progression.

In yeast, the location of a particular chromosome within the nucleus and its association with its sister chromatid following DNA replication are commonly assayed using arrays of the lactose-operator DNA binding site ($LacO_R$) and a GFP fusion to the DNA binding region of the *lac* repressor (GFP-LacI) (Figure 1, A and E). If the array is inserted into a telomeric region of the genome in a strain containing a NE marker, the distance between the chromosomal focus of GFP-LacI and the NE, as well as the nuclear diameter, can be measured, and each spot is assigned into one of three concentric zones of equal volume that approximates the position of the telomere within the nucleus (Figure 1A) (Hediger *et al.* 2002). If the array is integrated into a chromosomal region near the centromere, it can be used to assay cohesion between sister chromatids—the linkage between sisters resists chromosome separation (and that of the arrays) until the onset of anaphase, so a single focus is observed in metaphase-arrested cells if cohesion is maintained (Figure 1E) (Straight *et al.* 1996). Both assays have been used previously to show that the Mps3 N-terminus is required for telomere tethering and sister-chromatid cohesion (Bupp *et al.* 2007; Schober *et al.* 2009; Ghosh *et al.* 2012).

Here we show that deletion of *POM152* was unable to suppress the requirement for Mps3 function in either process. In wild-type cells, 67% of telomeric foci in S phase (scored based on bud morphology) were located in the outer zone of the nucleus, which is considered to be in contact with the NE (Figure 1, B and C) (Hediger *et al.* 2002). Cells lacking *POM152* had a small but statistically significant decrease in

telomere tethering (43% foci in zone 1), consistent with previous findings that NPC components affect the peripheral recruitment of chromosome ends (Galy *et al.* 2000; Therizols *et al.* 2006; Van de Vosse *et al.* 2013). However, if *MPS3* also was deleted, chromosomes assumed a random distribution (Figure 1, B and C). This loss of tethering in cells lacking *MPS3* correlated with a loss of telomeric silencing, which was assayed using an *ADE2* marker located at a truncated version of telomere VI-R. In wild-type cells, where telomeres were tethered, stochastic expression of *ADE2* led to the formation of red and white colonies after growth on plates containing limiting amounts of adenine (Figure 1D). A similar expression pattern was observed in *pom152Δ* cells, but *pom152Δ mps3Δ* cells appeared light pink to white in color, similar to *mps3Δ75–150* mutants, as a result of increased expression of *ADE2* at the truncated telomere (Figure 1D) (Bupp *et al.* 2007). In the cohesion assay, 79% of wild-type and 74% of *pom152Δ* cells maintained cohesion in a metaphase arrest (Figure 1, F and G). Only 63% *mps3Δ pom152Δ* cells established cohesion (Figure 1, F and G), which is similar to the amount of cohesion observed in *mps3Δ75–150* mutants (64%) (Ghosh *et al.* 2012). These data demonstrate that deletion of *POM152* does not suppress the requirement for *MPS3* in sister-chromatid cohesion, telomere tethering, or silencing during mitotic growth.

To determine whether *pom152Δ* suppresses the need for Mps3 in meiosis, we constructed a series of heterozygous and homozygous diploids containing *POM152* or *pom152Δ* and *MPS3* or *mps3Δ*. In the construction of these strains, we noticed that it was difficult to obtain diploids if both parental cells were of the *pom152Δ mps3Δ* genotype. This defect was suppressed by the addition of a covering plasmid containing *MPS3* but not *POM152* in one or both of the haploid parents. The covering plasmid could be lost in the diploid, indicating that *pom152Δ/pom152Δ mps3Δ/mps3Δ* diploids are viable, although they do show an increased rate of chromosome loss and a slight growth defect (Figure 1H; data not shown). These data support the recent finding from Rogers and Rose (2014) that Mps3 is required for karyogamy (nuclear fusion following mating) and that elimination of *POM152* cannot bypass this requirement. Sporulation of diploids showed that *POM152* deletion does not rescue Mps3 function during meiosis. Cells lacking both copies of *MPS3* were unable to form tetrads after 5 days in sporulation medium (Figure 1I). The sporulation frequency between wild-type (35 ± 2%) and *pom152Δ* homo- and heterozygotes (ranging from 23–30%) (Figure 1I) was only moderately decreased, indicating that deleting *POM152* had a minor effect on meiosis, sporulation, and/or germination. However, if *MPS3* is deleted, virtually no meiotic products are formed, including dyads or tetrads, pointing to an arrest early in the meiotic program (Figure 1I). Thus, although *pom152Δ* suppresses the essential function of Mps3 during mitosis, it is unable to bypass the need for Mps3 during meiosis and sporulation. Collectively, these data lend support to the idea that deletion of *POM152* specifically affects the SPB function of *MPS3* during mitotic growth.

A genome-wide screen for suppressors of mps3Δ

To better understand how the requirement for Mps3 at the SPB can be bypassed, we conducted a genome-wide screen for other deletions that can suppress the lethality of *mps3Δ*. Because the deletion collection of nonessential yeast genes was made in the BY strain background, we constructed a query strain containing *mps3Δ* covered by *MPS3* on a *URA3*-marked centromeric plasmid in this background for use in high-throughput studies (Figure 2, A and B). Following mating and diploid selection, the *pCEN-URA3-MPS3* covering plasmid was removed by two rounds of growth on 5-FOA, and then diploids were sporulated and haploids selected using markers engineered into the strain (see *Materials and Methods*). Because *MPS3* is essential for growth, only deletions that bypass the requirement for Mps3 function should be viable on plates that select for both *mps3Δ* and the gene knockout. Of the ~4900 deletion mutants in the collection, only 35 genes reproducibly (in three iterations of the screen) rescued *mps3Δ* cells (Table S1, Table S2, and Figure 2C). Thirteen deletions were along a region of chromosome *13* that contains an unknown suppressor of other essential genes (Copic *et al.* 2012), so these hits were not considered further (see Table S2 and *Materials and Methods* for a discussion of these genes).

To ensure that suppression in the remaining cases did not occur through a secondary mutation that cosegregated with *mps3Δ* or the deletion mutant, knockouts were made *de novo* in W303, a strain background commonly used in studies of SPB duplication. Of the remaining 22 deletions, only three hits, *pom152*Δ, *pom34Δ*, and *sec66Δ*, suppressed growth of *mps3Δ* mutants in W303 (Figure 2D). A single gene was not responsible for the strain-specific differences between W303 and BY that we observed for the other deletions because multiple outcrosses were required to convert a BY-like phenotype to a W303-like phenotype or vice versa (data not shown).

The robust suppression by *pom152Δ* in the genome-wide screen was consistent with our previous work showing that its elimination resulted in loss of Ndc1 from the NPC and increased Ndc1 binding at the SPB (Chen *et al.* 2014). *NDC1* overexpression and/or *pom152Δ* can suppress a number of conditional alleles in genes encoding SPB components (Chial *et al.* 1998; Araki *et al.* 2006; Jaspersen *et al.* 2006; Anderson *et al.* 2007; Sezen *et al.* 2009; Witkin *et al.* 2010), but elimination of *POM152* was only able to bypass deletions of *MPS3* or *MPS2* and not other membrane or half-bridge components of the SPB (Figure 2C; data not shown). Our observation that *pom152Δ* is unable to suppress the growth of *mps2Δ mps3Δ* double mutants suggests that Mps2 is required for *pom152Δ*-dependent bypass of *mps3Δ* and that Mps3 is required for *pom152Δ*-dependent bypass of *mps2Δ* (Figure 2E).

sec66Δ suppresses mps3Δ and mps2Δ

SEC66/SEC71/KAR7 encodes an integral membrane component of the Sec63 complex (Feldheim *et al.* 1993; Kurihara and Silver 1993; Brizzio *et al.* 1999). Together with the Sec61 translocon, the Sec63 complex is important for post-translational

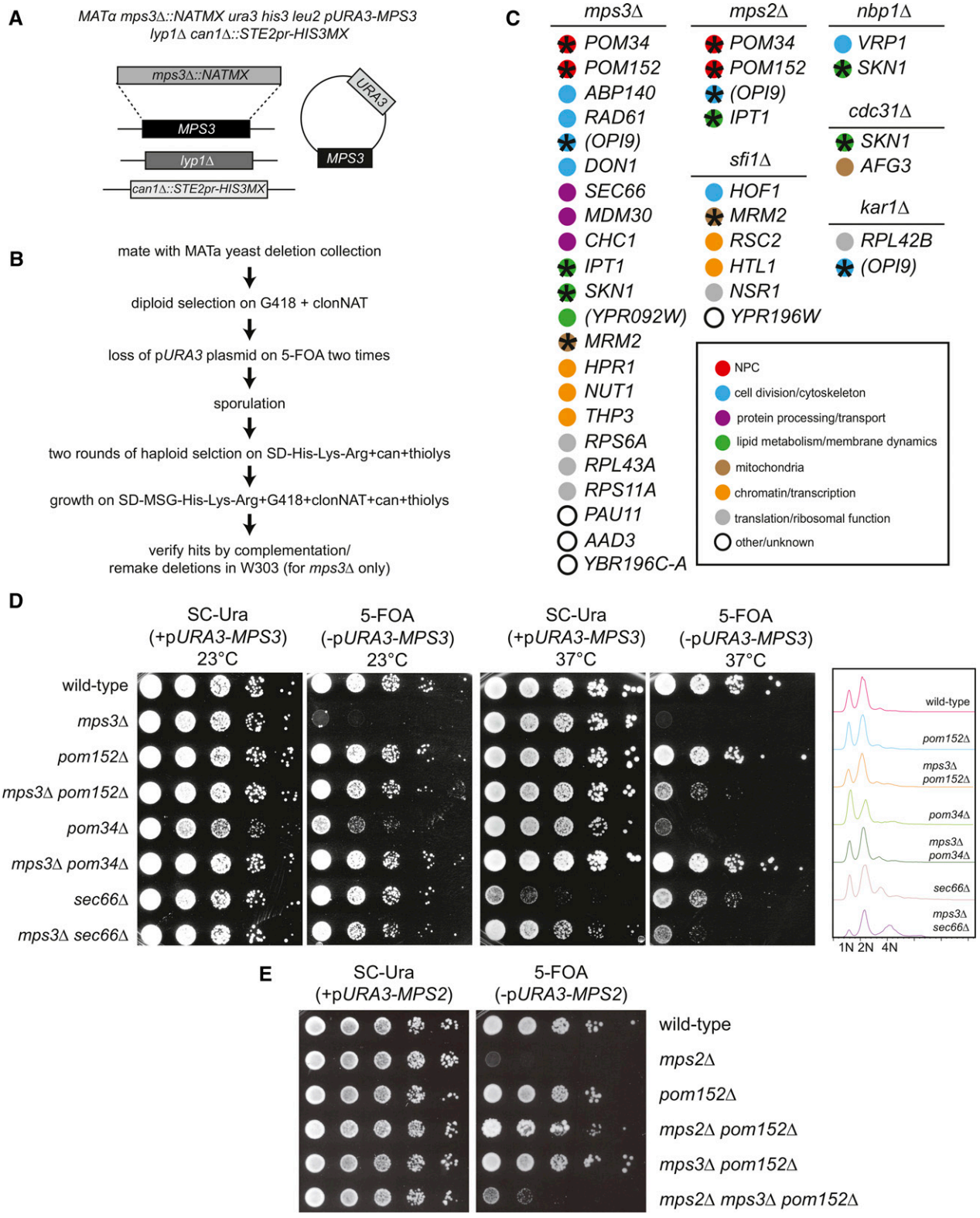

Figure 2 Suppressors of SPB deletions. (A) Schematic of the *mps3Δ* strain (SLJ1888) used for our suppressor screen. Genes encoding the lysine permease *LYP1* and the arginine permease *CAN1* were deleted in the query strain. This strain also contained *S. pombe his5+* (*HIS3MX*) expressed from the *MAT***a**-specific *STE2* promoter. After addition of a *URA3*-based covering plasmid containing a wild-type copy of *MPS3*, the genomic copy of *MPS3* was deleted using the *NATMX* marker. (B) Outline of screening strategy used for identification of suppressors. Query strains were mated to the *MAT***a** version of the yeast deletion collection, and diploids were selected on YPD + G418 + clonNAT. The *URA3*-marked plasmid was removed from the diploids by two rounds of growth on 5-FOA; then the diploids were sporulated. Haploids were selected by growth on SD-His-Lys-Arg + thialysine + canavanine; then cells containing both deletions were selected by addition of G418 + clonNAT. Because SPB genes are essential, most double-mutant

translocation of proteins into the ER (Figure 3A) (Park and Rapoport 2012; Ast and Schuldiner 2013; Mandon *et al.* 2013). Previous studies showed that *SEC66* is nonessential for growth at 25 and 30°, but *sec66Δ* cells show reduced growth at 37° (Feldheim *et al.* 1993; Kurihara and Silver 1993; Fang and Green 1994). We found this temperature sensitivity to be largely dependent on strain background (Figure 2D, Figure 3, B and C, and Figure S1). Genetic or physical interactions between Sec66 and SPB components have not been reported, and Sec66 does not localize to the SPB (Figure 3E). *sec66Δ* was not identified as a suppressor of other SPB deletion mutants in our genome-wide screens (Figure 2C); however, direct testing in the W303 strain background showed that *sec66Δ* bypassed the requirement for *mps2Δ* at 23° in addition to *mps3Δ* at all temperatures, but it had no effect on growth of other SPB deletions (Figure 3, B and C, and Figure S1). Unlike *mps3Δ pom152Δ* or *mps3Δ pom34Δ* cells that remained haploid, *mps3Δ sec66Δ* mutants showed a partial increase in ploidy, and *mps2Δ sec66Δ* mutants completely diploidized (Figure 2D; data not shown). This suggests that Mps3 and Mps2 have functions that are not or are incompletely bypassed by deletion of *SEC66*. Alternatively, given that *sec66Δ* alone shows a small 4N peak (Figure 2D), this change in chromosome content may be associated with a mitotic defect in the deletion in *SEC66*. Our observation that deletion of *SEC66* and *POM152* did not have additive effects on the growth of *mps3Δ* is most consistent with the idea that Sec66 and Pom152 are in the same pathway, although we cannot completely rule out the idea of a threshold effect because *mps2Δ sec66Δ pom152Δ* cells grew better than *mps2Δ sec66Δ* cells (Figure 3, B and C). Elimination of other nonessential components of the Sec61 (*SBH1*) or Sec63 (*SEC72*) complex did not suppress *mps3Δ*, nor did deletion of the Sec61 homolog *SSH1* (Figure 3D). Conditional mutants in *SEC61* and *SEC63* also did not bypass *mps3-Δ* (data not shown), lending evidence to the idea that Sec66 is specifically involved in the control of SPB duplication via a pathway related to Mps3.

Characterization of SEC66

Previous work showed that cells lacking *SEC66* have defects in translocation/insertion of a subset of proteins at the ER membrane, including the ER resident protein Kar2/BiP and the secreted proteins invertase/Suc2, α-factor, and vacuolar carboxy peptidase Y (Feldheim *et al.* 1993). A recent study using ribosome profiling implicated Sec66 in processing and ER docking of proteins with a looped signal sequence (Jan *et al.* 2014). Although nucleoporins and SPB components were not among the list of genes controlled by Sec66 and lack these sequence motifs, one could envision that loss of Sec66 function partially blocks ER import or folding of proteins needed directly or indirectly for SPB or NPC function, perhaps fully or partially mimicking *pom152Δ* and/or *pom34Δ*. Therefore, we examined NPC distribution, nucleocytoplamic transport, SPB duplication, and spindle assembly in wild-type and *sec66Δ* cells.

Fusions between GFP and the nucleoporins Nic96, Nup192, Nup188, and Nup49 were created by PCR at endogenous loci in a strain containing the ER reporter HDEL-dsRed (a Kar2 signal sequence followed by dsRed and the yeast ER retrieval sequence HDEL) (Rossanese *et al.* 2001). The cytoplasmic signal of HDEL-dsRed was slightly increased in *sec66Δ* mutants compared to wild-type cells, which could be due to partial defects in its ER translocation because previous studies showed impaired import of full-length Kar2 in cells with mutant versions of *SEC66* (Figure 4A) (Green *et al.* 1992; Feldheim *et al.* 1993; Kurihara and Silver 1993). NPC assembly defects often manifest as foci of one or more nucleoporins in the nucleus or cytoplasm. The lack of cytoplasmic or nuclear Nic96-GFP, Nup192-GFP, Nup188-GFP, and GFP-Nup49 foci in *sec66Δ* mutants suggests that removal of *SEC66* does not result in major defects in NPC assembly, even if cells were shifted to 37° for 4 hr (Figure 4A and Figure S2A; data not shown). Wild-type and *sec66Δ* cells showed similar nuclear sizes, and NPCs were evenly distributed over the surface of the NE. To confirm that NPCs were intact and functional, we analyzed nucleocytoplasmic transport with a series of reporters containing nuclear localization sequences (NLSs) and/or nuclear export sequences (NESs). Shown in Figure 4 (B and C) is the steady-state distribution of the cNLS-GFP2 and rgNLS-NES^{mut}-GFP2 reporters that use the Kap60/Kap95 and Kap104 pathways, respectively (Stade *et al.* 1997; Lee and Aitchison 1999; Chook and Blobel 2001). A minor transport defect for cNLS-GFP2, but not rgNLS-GFP2, was observed in *mps3Δ sec66Δ* cells, but in cells lacking *SEC66* alone, the distribution of reporters was unaffected, similar to wild-type and *pom152Δ pom34Δ* cells (Miao *et al.* 2006). These data suggest that *sec66Δ* alone does not result in major defects in NPC structure and transport.

combinations are lethal, so suppressors were easily identified by visual inspection of the plates. Potential hits were further verified by random sporulation, complementation, and, in the case of *mps3Δ*, reconstruction of the deletions in W303. (C) Deletions that suppressed growth of the indicated SPB gene in at least two or three independent screens are listed in groups based on their proposed function and localization, as reported in the Saccharomyces Genome Database (with the exception of deletions in a small region of chromosome *13*, which are listed in Table S2; see *Materials and Methods* for a discussion of these hits). Dubious ORFs are in parentheses. An asterisk indicates that the gene was identified as a suppressor of more than one SPB deletion mutant. (D) Tenfold serial dilution of cells on SC-Ura or 5-FOA at 23 or 37° shows that *pom152Δ*, *pom34Δ*, and *sec66Δ* suppress *mps3Δ* lethality in W303. Flow cytometric analysis of DNA content of cells grown at 30° shows the ploidy of cells lacking a covering plasmid. Haploid, 1N and 2N peaks; diploid, 2N and 4N peaks. Some isolates of *sec66Δ* show temperature-sensitive growth phenotypes, as reported previously, and have a fraction of cells with increased ploidy. (E) W303-derived cells containing *pURA3-MPS2* and the indicated deletions were grown in YPD, serially diluted 10-fold, spotted onto SC-Ura or 5-FOA, and incubated for 3 days at 23°.

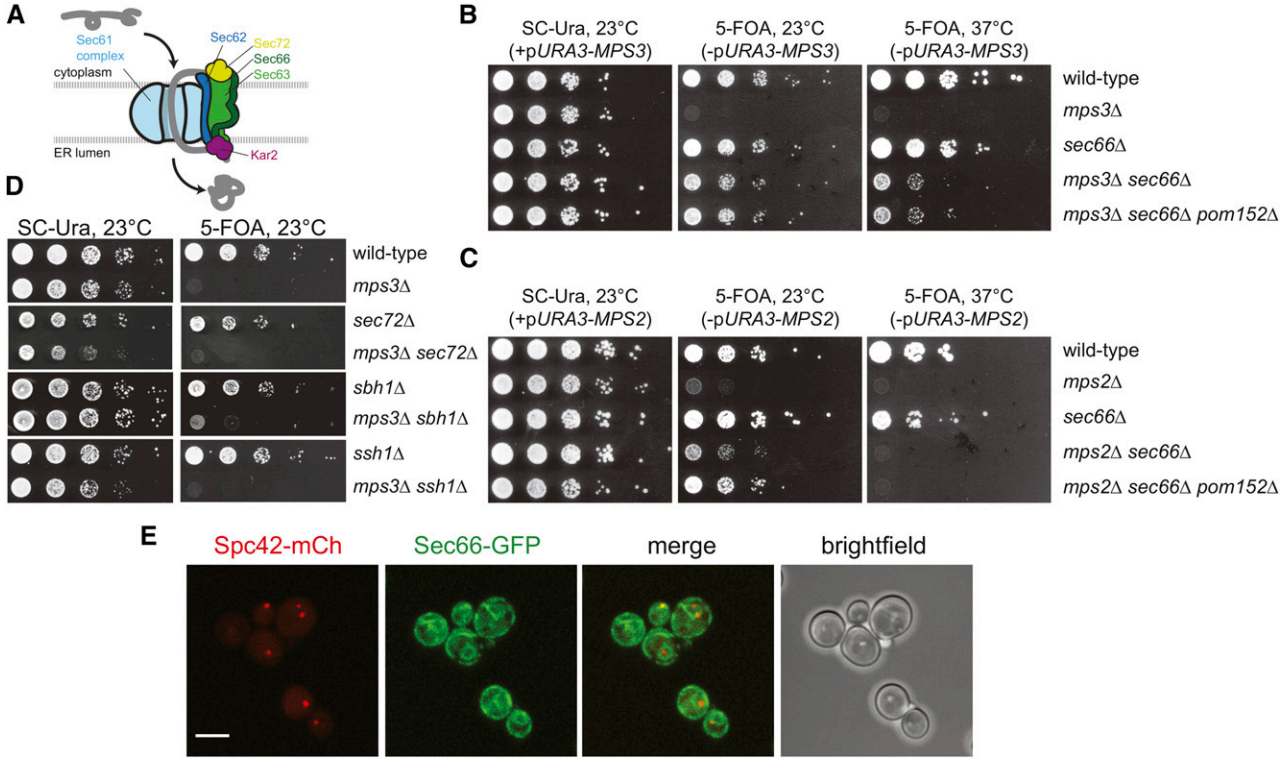

Figure 3 Deletion of *SEC66* bypasses the requirement for *MPS3* and *MPS2*. (A) Schematic of the heterotrimeric Sec61 complex (Sec61, Sss1, and Sbh1), which forms a channel in the ER membrane. Post-translational translocation of proteins (depicted in gray) also requires Sec62, the Sec63 complex (Sec63, Sec66, and Sec72), and Kar2. Yeast has a second Sec61-like complex composed of Ssh1, Sss1, and Sbh2, which is not shown. (B and C) W303-derived cells containing either a *pURA3-MPS3* (B) or a *pURA3-MPS2* (C) plasmid and the deletions shown were grown in YPD, serially diluted 10-fold, and spotted onto SC-Ura or 5-FOA. Plates were incubated at 23° for 3 days or 37° for 2 days. (D) The nonessential subunits of the Sec61 (*sbh1Δ*) and Sec63 (*sec72Δ*) complexes as well as Ssh1 (*ssh1Δ*; *sbh2Δ* was not tested) were combined with *mps3Δ* and tested for their ability to rescue growth in a dilution assay. Plates grown at 23° are shown, but no suppression was observed at any temperature. (E) Localization of Sec66-GFP in SLJ10508, a strain containing the SPB marker Spc42-mCherry. Bar, 2 μm.

Comparison of the transcriptome of wild-type and *sec66Δ* cells grown at 23° showed no difference in the expression levels of SPB or NPC genes, and machinery involved in protein folding or quality control was not induced, including components of the unfolded protein and stress-response pathways (Figure 4D and Table S3). Among the transcripts downregulated in *sec66Δ* compared to wild-type cells were a number of dubious ORFs (26 of 91), many of which appear to overlap with genes encoding ribosome subunits (11 of 26, 34.6% compared to a genome frequency of 5.5%). Most, but not all, of the dubious ORF transcripts are located on the noncoding strand and may represent antisense transcripts. However, decreased levels of the overlapping protein-coding gene were not observed, so the biological function and origin of the dubious ORF RNA were not investigated further (Figure S2B).

Examination of SPBs and microtubules using Spc42-mCherry and GFP-Tub1 in asynchronously grown cells revealed that a significant fraction of *sec66Δ* mutants assembled bipolar metaphase and anaphase spindles that were indistinguishable from wild-type spindles (Figure 4, E and F). However, broken spindles with microtubules from each SPB that do not overlap were observed in 12% (n = 102) of *sec66Δ* mutants *vs.* 4% (n = 105) of wild-type cells. Monopolar spindles in which a single SPB nucleates nuclear microtubules also were seen in 7% (n = 102) of *sec66Δ* cells compared to <1% (n = 105) of wild-type cells. The same or more severe spindle defects were observed in cells lacking *SEC72* and in temperature-sensitive mutants of *SEC63*, an essential subunit of the Sec63 complex (Figure 4, E and F, and Figure S3). Spindles within the bud and multipolar spindles were seen, particularly in *sec63–104* at both 23 and 37°, but no accumulation of cells in mitosis was detected either by flow cytometric analysis of DNA content or by budding index (Figure S3). Thus, perturbation of Sec63 complex function leads to spindle defects similar to other components of the secretory pathway (Winey *et al.* 1991; Duden *et al.* 1994; Yu *et al.* 2006). However, given that suppression is specific to *sec66Δ* (Figure 3D; data not shown), it is unlikely that the role of the Sec63 complex in spindle assembly or maintenance is related to the bypass pathway of *MPS2* and *MPS3*.

Elimination of SEC66 decreases Pom152 levels

Pom34 and Pom152 are integral membrane proteins that are presumably inserted into the ER via the Sec61 translocon together with the Sec63 complex (Wozniak *et al.* 1994;

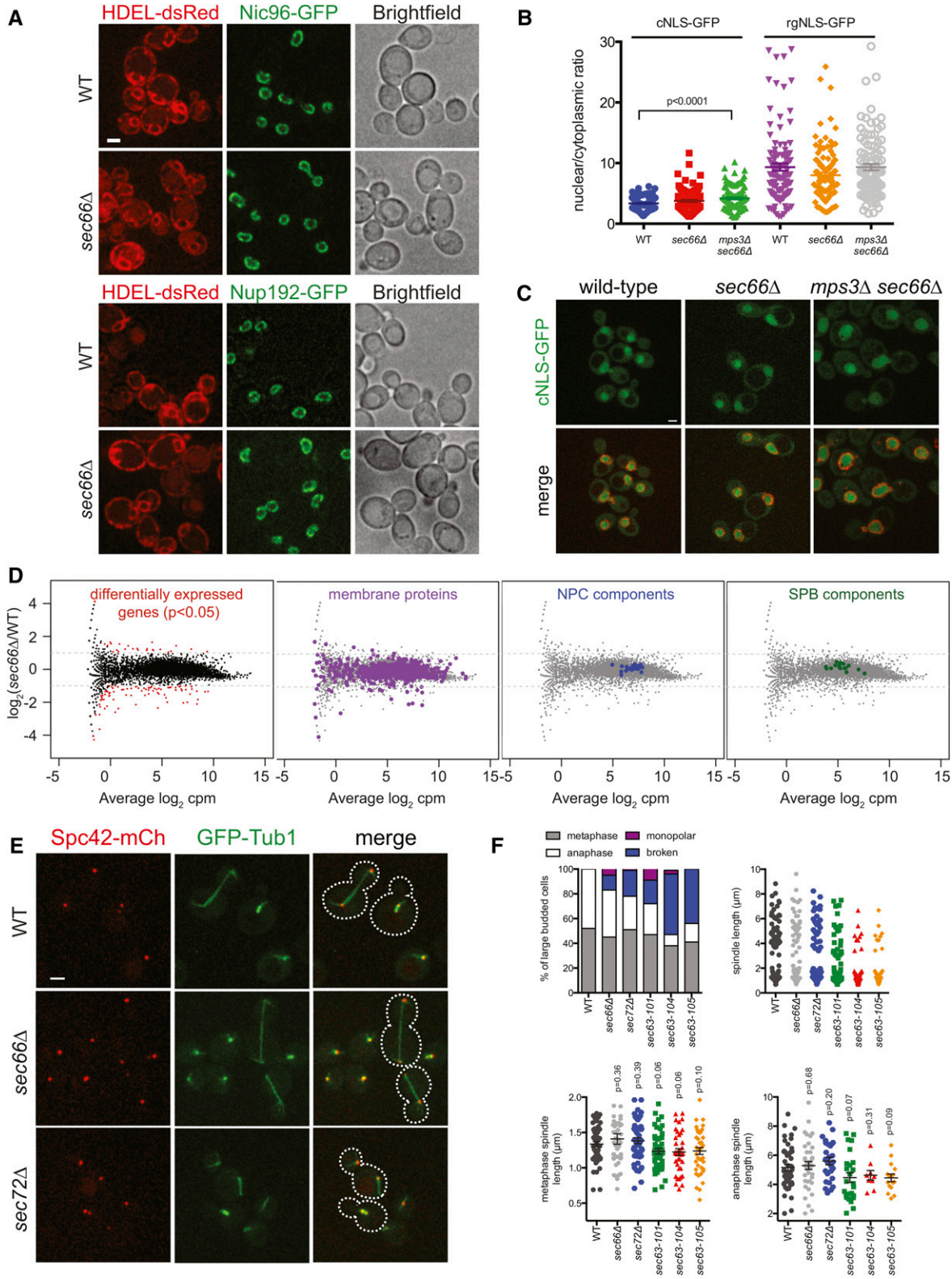

Figure 4 Characterization of NPCs and SPBs in cells lacking *SEC66*. (A) Wild-type and *sec66Δ* cells containing the ER marker HDEL-dsRed (red) and the NPC subunits Nic96-GFP (green, top panels) or Nup192-GFP (green, bottom panels) were grown at 30° and imaged. Bar, 2 μm. (B and C) Wild-type, *sec66Δ*, and *mps3Δ sec66Δ* cells containing Ndc1-mCherry (red) and the nuclear transport reporters cNLS-GFP (green) or rgNLS-GFP (not shown) were imaged, and the intensity of the reporter in the nucleus and cytoplasm was quantitated in each cell ($n > 100$). The long bar shows the average ratio of nuclear to cytoplasmic signal, and the shorter bars show SEM. *P*-values were calculated using the Student's *t*-test; only localization of cNLS-GFP in *mps3Δ sec66Δ* cells was statistically different from that of wild-type cells, as indicated. Bar, 2 μm. (D) Differentially expressed genes in wild-type (SLJ173)

Tcheperegine *et al.* 1999; Rout *et al.* 2000; Miao *et al.* 2006). Therefore, Sec66 may inhibit SPB duplication by altering the levels of Pom152 or Pom34, which would partially or completely mimic *pom152Δ* or *pom34Δ*. To test this idea, we fused the endogenous copy of *POM152* or *POM34* to YFP in wild-type, *sec66Δ*, and *mps3Δ sec66Δ* cells. Western blotting showed an increase in levels of Pom34-YFP in both *sec66Δ* and *mps3Δ sec66Δ* cells compared to wild-type cells, but analysis of its localization showed little change in the amount of Pom34-YFP at the NE (Figure 5, A–C). In contrast, Pom152-YFP levels decreased by over 50% in both assays in *sec66Δ* and *mps3Δ sec66Δ* cells compared to wild-type cells (Figure 5, A–C).

To test whether *sec66Δ* suppresses the growth of *mps3Δ* mutants via downregulation of Pom152, we added extra *POM152* to cells using a 2-μm plasmid. Overexpression of *POM152*, but not *POM34*, exacerbated growth of *mps3Δ sec66Δ* mutants, particularly at 37°, but did not affect the growth of wild-type cells (Figure 5D). A similar phenotype was observed if *POM152* was overproduced using the strong constitutive *GAL1/10* promoter (Figure 5E). Taken together, these observations suggest that Sec66 is required to maintain wild-type levels of Pom152 in the cell and that a decrease in Pom152 levels is at least partially responsible for the ability of *sec66Δ* to bypass the requirement for Mps3.

Sec66 effects at the SPB are independent of Ndc1

Previously, we proposed that a shift in Ndc1 binding from the NPC to the SPB underlay the ability of *pom152Δ* to bypass the requirement for Mps3. This conclusion was based in part on our finding that deletion of *POM152* resulted in decreased amounts of NPC-associated Ndc1 and increased Ndc1 levels at the SPB (Chen *et al.* 2014). Thus, we anticipated finding more Ndc1 at the SPB in *sec66Δ* mutants as a result of decreased Pom152 levels (Figure 5, A–C).

Quantitative Western blotting of Ndc1-GFP in wild-type and *sec66Δ* cells showed little change in total intracellular levels of Ndc1 (Figure 5C), and imaging showed that the distribution of protein on the NE and SPB also was similar (Figure 6, A–C). To study the spatial relationship between Ndc1 and Nbp1 at the SPB, we used acceptor-photobleaching FRET. In this method of FRET, the fluorescence intensity of the FRET donor is measured before and after bleaching the FRET acceptor. If energy transfer occurs between the FRET pairs, fluorescence of the FRET donor should increase after bleaching of the acceptor, which is expressed in a FRET efficiency score (see *Materials and Methods*). Because molecules must be in close proximity for the energy transfer to occur, FRET efficiency is related to the distance between donor and acceptor. Two SPB components (Spc42-mTurquoise2 and Cnm67-YFP) previously shown to exhibit high FRET gave 11.0 ± 1.0% (n = 159) FRET efficiency in our system (Muller *et al.* 2005). In contrast, if molecules are unable to transfer energy, no change in fluorescence of the FRET donor should be observed after bleaching. YFP-Spc110-mTurquoise2 exhibits 0.4 ± 1.1% (n = 79) FRET owing to the fact that the N- and C-termini of Spc110 are separated by 600–800 Å (Muller *et al.* 2005). Using Nbp1-mTurquoise2 as the donor and Ndc1-YFP as the acceptor, we observed 4.8 ± 1.1% (n = 113) FRET at the SPB in wild-type cells and 6.5 ± 1.8% (n = 79) FRET in *sec66Δ* cells, a change that was not statistically significant. This result suggests that Ndc1 and Nbp1 are in close proximity at the SPB and that their location is unchanged on loss of Sec66.

In *mps3Δ sec66Δ* mutants, several notable differences between wild-type and *sec66Δ* cells were observed. First, although all strains were haploid at the beginning of our experiment, the heterogeneity in nuclear (Figure 6, A and B) and cell size (not shown) in *mps3Δ sec66Δ* suggested that at least some fraction of cells diploidized during the course of our experiment. Because SPB and nuclear size scale with ploidy (Byers and Goetsch 1974; Bullitt *et al.* 1997; Jorgensen *et al.* 2007), levels of Ndc1-YFP at both the SPB and NE were higher in a fraction of the double-mutant cells compared to wild-type and *sec66Δ* cells (Figure 6, A and B). However, the ratio of Ndc1-YFP at the SPB and NE, using values derived from each cell, showed that the distribution of Ndc1 is largely unaffected (Figure 6B). Second, levels of Nbp1-mTurquoise2 at the SPB were reduced in *mps3Δ sec66Δ* cells compared to wild-type or *sec66Δ* cells (Figure 6, A and C). Despite this reduction, FRET between Ndc1-YFP and Nbp1-mTurquoise2 in *mps3Δ sec66Δ* cells (6.5 ± 2.2%, n = 114) is virtually indistinguishable from that in *sec66Δ* cells and is not statistically different from wild-type cells. The fact that FRET does not decrease despite a reduction in levels of the Nbp1 donor in *mps3Δ sec66Δ* cells suggests that Nbp1 is the limiting factor at the SPB (Figure 6E), although it is formally possible that conformational differences between

vs. *sec66Δ* (SLJ5281) cells are shown in red in the plot, with average counts on the *x*-axis and the change in expression on the *y*-axis. Dashed lines at −1 and 1 indicate a twofold change in expression. The position of membrane and NPC- and SPB-encoding genes within the expression data are also shown. (E and F) Wild-type (SLJ6834), *sec66Δ* (SLJ10759), *sec72Δ* (SLJ10775), *sec63–101* (SLJ10773), *sec63–104* (SLJ10774), and *sec63–105* (SLJ10807) cells containing Spc42-mCherry (red) and GFP-Tub1 (green) to visualize the SPB and microtubules, respectively, were grown to log phase at 23° and imaged. Examples images of large budded cells are shown in E, with dashed lines drawn based on bright-field images. Bar, 2 μm. (F) Spindle morphology was analyzed in at least 100 large budded cells of each genotype. Monopolar spindles (large budded cells containing a single SPB or containing two SPBs, only one of which nucleates nuclear microtubules) and broken spindles (large budded cells with two separated SPBs that contain nonoverlapping arrays of nuclear microtubules) were observed. The percentage of metaphase and anaphase spindles was determined using the natural gap in spindle length that occurred at 2 μm in all strains. Average length is shown by the long bar, and the shorter bars show SEM. *P*-values calculated using the Student's *t*-test are listed. While none are statistically different from wild-type cells, the fraction of anaphase cells with intact spindles decreased particularly in *sec63–104* and *sec63–105* cells.

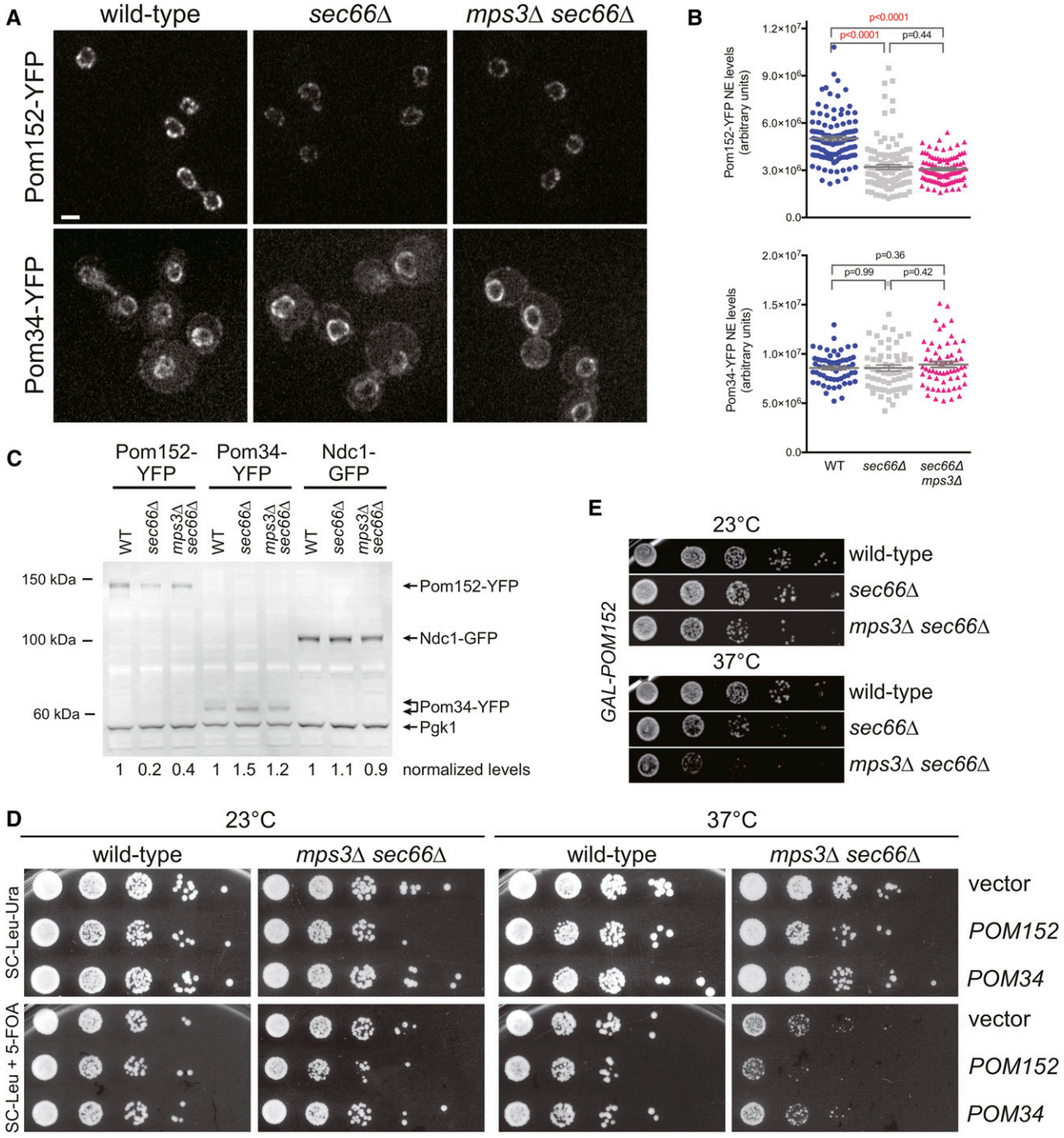

Figure 5 Pom152 protein levels are reduced in cells lacking *SEC66*. Mid-log phase cultures of wild-type (SLJ8167, SLJ7824), *sec66Δ* (SLJ8168, SLJ7854), and *mps3Δ sec66Δ* (SLJ8339, SLJ7895) cells containing Pom152-YFP or Pom34-YFP grown in SC-complete medium at 30° were examined. (A) Projection images of three Z-slices in the center of the nucleus showing NE localization. Bar, 2 μm. (B) Levels of Pom152-YFP or Pom34-YFP were quantitated as described in *Materials and Methods*. For the 60 cells examined, the total fluorescence intensity is shown in arbitrary fluorescence units. The average fluorescence intensity is indicated by the long bar, and the shorter bars show SEM. *P*-values calculated by Student's *t*-test are listed. (C) Extracts were prepared from the previous strains, Ndc1-GFP (SLJ7936, SLJ7937, and SLJ7938) and wild type (SLJ1070). Western blotting using anti-GFP antibodies was used to determine the total level of Pom152-YFP, Pom34-YFP, or Ndc1-GFP in the cell. Pgk1 is a loading control. Samples were normalized so that wild type cells had a value of 1. Molecular weight markers are shown on the left. (D) Wild-type (SLJ8666) and *mps3Δ sec66Δ* (SLJ8669) cells containing *pURA3-MPS3* were transformed with an empty *LEU2*-marked 2μ plasmid (vector) or version containing the indicated gene. Tenfold serial dilutions were spotted onto SC-Ura-Leu or SC-Leu containing 5-FOA, and plates were incubated for 2 days at 37° or 3 days at 23°. (E) Wild-type (SLJ9253), *sec66Δ* (SLJ9259), and *mps3Δ sec66Δ* (SLJ9262) cells containing *GAL-POM152* were serially diluted 10-fold, spotted onto plates containing 2% raffinose and 0.5% galactose, and incubated for 2 days at 37° or 3 days at 23°.

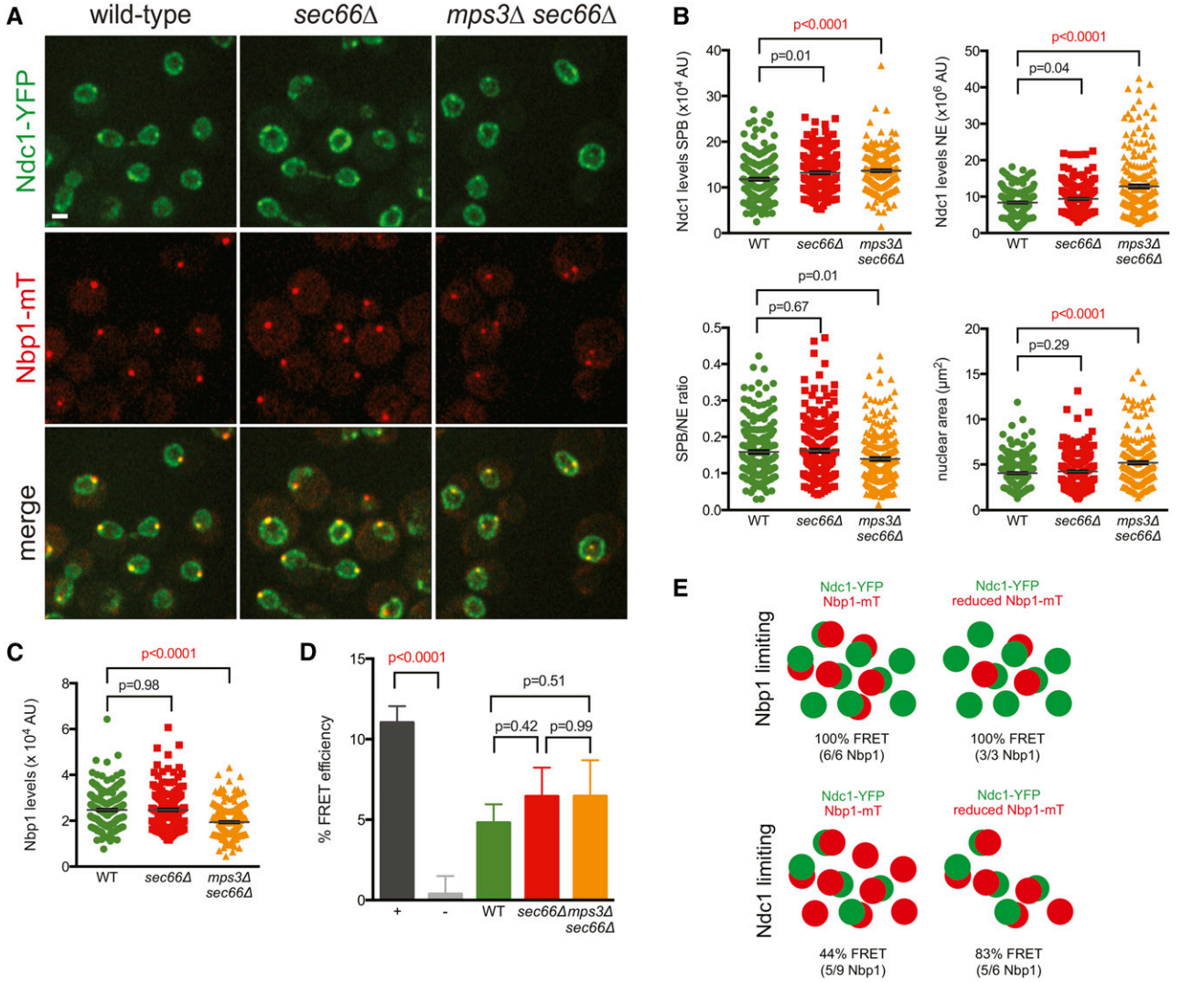

Figure 6 Ndc1 distribution is Sec66 independent. Wild-type (SLJ9356), *sec66Δ* (SLJ9357), and *mps3Δ sec66Δ* (SLJ10808) strains expressing *NDC1-YFP* and *NBP1-mTurquoise2* from their endogenous loci were grown to mid-log phase in SC Complete medium at 30° and examined. (A) Sum projection images of five Z-slices in the center of the nucleus showing Ndc1-YFP (green) at the NE and the SPB and Nbp1-mTurquoise2 (red) at the SPB. Bar, 2 μm. (B and C) Levels (in arbitrary fluorescence units) of Ndc1-YFP at the SPB and NE and Nbp1-mTurquoise2 levels at the SPB were quantitated as described in *Materials and Methods*. The ratio of Ndc1-YFP at the SPB/NE also was calculated for each cell, along with the nuclear area, using Ndc1-YFP at the NE. Long bars depict average values, while shorter bars show SEM. *P*-values compared with wild type were calculated using Student's *t*-test and are listed. (D) Binding between Ndc1-YFP and Nbp1-mTurquoise2 was analyzed at the SPB using acceptor photobleaching FRET in wild-type (SLJ9356), *sec66Δ* (SLJ9357), or *mps3Δ sec66Δ* (SLJ10808) cells. As a positive control, FRET was measured in a strain containing Spc42-mTurquoise2 and Cnm67-YFP (SLJ8173); as a negative control, FRET was assayed in a strain in which *SPC110* was tagged at its N-terminus with YFP and its C-terminus with mTurquoise2 (SLJ9012). Average FRET efficiency is plotted; error bars are SEM from at least 35 cells. *P*-values were calculated using the Student's *t*-test and are shown. (E) In acceptor-photobleaching FRET, a reduction in donor levels (Nbp1-mTurquoise2) does not affect the FRET efficiency if the donor (Nbp1) is limiting. However, reduced levels of the donor (Nbp1-mTurquoise2) should result in increased FRET efficiency if the acceptor (Ndc1-YFP) is limiting. Note that this simplified model assumes that all molecules are capable of FRET, and it does not account for conformational changes that also may affect FRET efficiency.

Ndc1-YFP and Nbp1-mTurquoise2, rather than changes in the number of bound molecules, account for FRET observed. Third, the observation that Ndc1-YFP/Ndc1-GFP levels at the SPB are not decreased in *mps3Δ sec66Δ* cells suggests that Ndc1 binds to additional SPB components besides Nbp1. While Sec66 may act by lowering Pom152 levels, the decreased dosage of Pom152 does not alter Ndc1 distribution and thus does not phenocopy *pom152Δ* (Chen *et al.* 2014). This suggests that the mechanism of suppression in *sec66Δ* cells is Ndc1 independent and that Pom152 may affect the SPB in more than one way.

Reduction of Pom152 is able to bypass Mps3 function

To test the idea that Pom152 dosage is important for SPB duplication, we compared the effects of removing one or both copies of *POM152* in diploid cells lacking *MPS3*. At 23 or 30°,

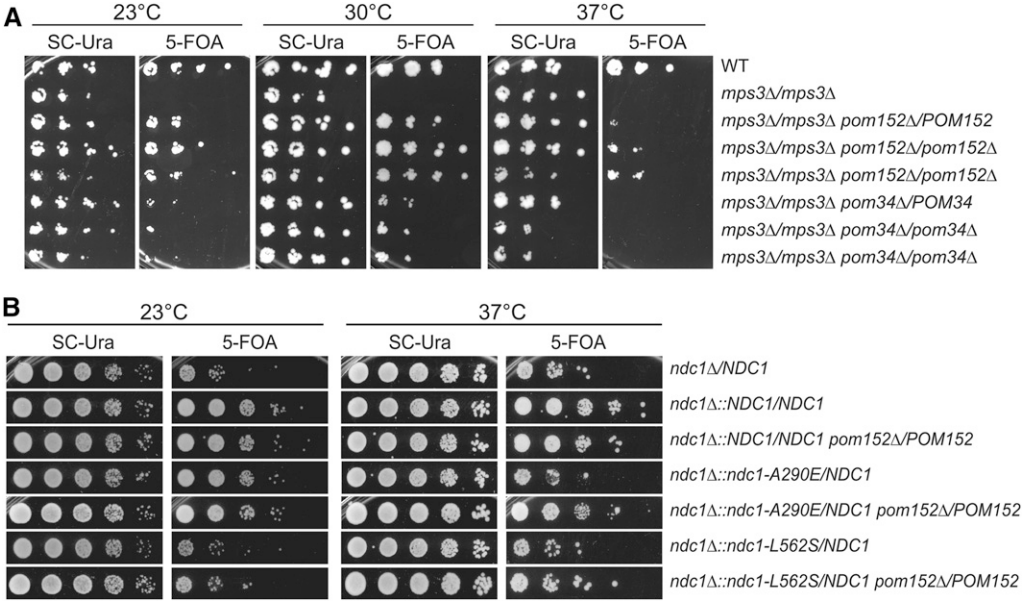

Figure 7 Pom152 dosage-dependent suppression of SPB mutants. (A) The ability of a hetero- or homozygous deletion of *POM152* or *POM34* was tested for its ability to rescue the growth defect of diploid strains lacking *MPS3* by plating 10-fold serial dilutions of cells on SC-Ura (which selects for the *pURA3-MPS3* plasmid) or 5-FOA (which selects for loss of the plasmid). Growth at 23° (4 days), 30° (4 days), or 37° (3 days) is compared to a wild-type diploid. (B) Similarly, the growth of diploid cells containing the indicated combinations of *NDC1* and *POM152* alleles was compared.

elimination of one copy of *POM152*, which decreases the dosage of the gene by 50%, is able to suppress the growth arrest of *mps3Δ/mps3Δ* cells (Figure 7A). The effect is weaker at 37° in both hetero- and homozygous *pom152Δ* cells, but the dosage seems to be Pom152 specific. Elimination of one copy of *POM34* produced an identical phenotype as deletion of both copies—suppression of growth at 30° but not at 23 or 37°. Deletion of one copy of *POM152* is unable to suppress the haploinsufficiency of *ndc1-L562S* (Figure 7B), a mutant allele of *NDC1* that displays Pom152-dependent binding to Mps3 (Chen *et al.* 2014). These findings are consistent with the idea that Pom152 levels play a key role in the control of SPB duplication independent of Ndc1.

Discussion

Because the SPB is the sole site of microtubule nucleation in budding yeast, virtually all components of the SPB are essential for viability. Therefore, it is somewhat surprising that bypass suppressors of SPB deletion mutants were recovered. Although previous work revealed genetic connections between the NPC and the SPB (Chial *et al.* 1998; Sezen *et al.* 2009; Greenland *et al.* 2010; Witkin *et al.* 2010; Friederichs *et al.* 2011; Casey *et al.* 2012; Chen *et al.* 2014), our work is the first to show that Sec66 plays a role in SPB duplication. Based on the fact that deletion of *SEC66* bypasses the requirement for *MPS3* and, to a lesser extent, *MPS2*, it seems that in wild-type cells, Sec66 functions to inhibit SPB duplication.

Our observation that deletion of *POM152* and *SEC66* did not have additive effects on growth of *mps2Δ* or *mps3Δ* cells suggests that Sec66 is likely acting in the same pathway as Pom152. However, unlike cells lacking *POM152* (Chen *et al.* 2014), the distribution of Ndc1 between the NPC and the SPB was largely unaffected. Perhaps this is because *sec66Δ* mutants have some Pom152 protein (~50% reduction from wild-type cells compared with 100% in *pom152Δ* cells based on gene dosage). The fact that Ndc1 distribution is unchanged and that overproduction of Pom152 alone is detrimental to *mps3Δ sec66Δ* mutants under conditions where it does not affect the growth of wild-type or *sec66Δ* cells leads us to hypothesize that Pom152 has a direct role in blocking SPB duplication and that simply lowering levels is adequate to overcome the requirement for certain SPB components. This mechanism of suppression is not as efficient as *pom152Δ*, which not only removes Pom152 from the cell but also causes a redistribution of Ndc1 (Chen *et al.* 2014). Unlike *mps3Δ pom152Δ* cells that are stable haploids with no obvious SPB abnormalities (Witkin *et al.* 2012), *mps3Δ sec66Δ* cells exhibit a partial increase in ploidy, and *mps2Δ sec66Δ* mutants spontaneously diploidize, which is commonly observed in cells with SPB duplication defects.

Multiple models have been proposed to explain the genetic relationship between NPCs and the SPB, including the idea that NPC components such as Pom152 may directly inhibit SPB duplication. Pom152 has been recovered in purified SPB preparations, and NPCs are often observed by EM in the vicinity of the duplicating SPB (Wigge *et al.* 1998; Adams and Kilmartin 1999). The model of Pom152-dependent inhibition predicts that more Nbp1 should localize to the SPB in *mps3Δ sec66Δ* mutants than in wild-type cells owing to reduced levels of Pom152. However, reduced levels of Nbp1 may have been observed because Mps3 is required to stabilize Nbp1 at the SPB. Mps3 and Nbp1 copurify, and overexpression of *NBP1* is able to restore growth to certain *MPS3* mutants (Jaspersen *et al.* 2006; Kupke *et al.* 2011). It is unknown whether the stability of Nbp1 is controlled or whether Mps3 and Nbp1 form a SPB-associated complex. Reduced levels of Pom152 also may result in decreased transport of Nbp1 into the nucleus or affect NE lipids (Friederichs *et al.* 2011; Kupke *et al.* 2011; Jaspersen and Ghosh 2012). Future studies will be

required to elucidate the bypass mechanism, but our FRET, together with recent super-resolution imaging data (Burns *et al.* 2015), lends evidence to the idea that Nbp1 is a key SPB insertion factor.

Sec66 is a nonessential subunit of the budding yeast Sec63 complex, which is involved in targeting and translocation of a subset of proteins into the ER (Feldheim *et al.* 1993; Kurihara and Silver 1993; Brizzio *et al.* 1999). Sec66 might be involved in the membrane insertion of Pom152, but it is unclear why other components of the Sec63 complex, including temperature-sensitive *sec63* alleles and *sec72Δ*, do not share the same ability to rescue *mps3Δ* or *mps2Δ*. We favor the idea that Sec66 plays a specialized role in the control of SPB duplication via Pom152 that may be independent of its role as a component of the Sec63 complex. This might explain why *SEC66* is present only in lower eukaryotes that typically undergo a closed mitosis in which the SPB must assemble into the NE. Sec66 together with Pom152 may control events needed for SPB insertion into the membrane. This function would be similar, but not identical, to post-translational assembly of integral membrane proteins at the ER (Shao and Hegde 2011) and suggests that the primary role of Mps2 and Mps3 during SPB duplication is to facilitate membrane insertion of the newly duplicated pole.

While it is not surprising that bypass suppressors of *MPS3* such as *pom152Δ* do not rescue the function of Mps3 in telomere tethering or sister-chromatid cohesion, it is unclear why deletion of *POM152* is unable to rescue *mps3Δ* during meiosis because the SPB is key to the formation of the meiosis I and II spindles (Moens and Rapport 1971). Therefore, it seems likely that Mps3 has an essential meiotic function not suppressed by *pom152Δ*, such as its role in meiotic chromosome movement or linking SPBs prior to meiosis I (Conrad *et al.* 2007, 2008; Koszul *et al.* 2008; Lee *et al.* 2012; Li *et al.* 2015).

Acknowledgments

We are grateful to Sue Biggins, Trisha Davis, and Pam Silver for sharing strains and plasmids; to Suman Ghosh, who assisted in strain construction and telomere analysis in Figure 1B; to Lynn Stoltz for help with dilution assays; and to Christine Smoyer, who localized Sec66. We thank David Obeso for helpful discussions and comments on the manuscript. S.L.J. is supported by the Stowers Institute for Medical Research and the American Cancer Society (RSG-11-030-01-CSM).

Literature Cited

Adams, I. R., and J. V. Kilmartin, 1999 Localization of core spindle pole body (SPB) components during SPB duplication in Saccharomyces cerevisiae. J. Cell Biol. 145: 809–823.

Aitchison, J. D., and M. P. Rout, 2012 The yeast nuclear pore complex and transport through it. Genetics 190: 855–883.

Anderson, V. E., J. Prudden, S. Prochnik, T. H. Giddings, Jr., and K. G. Hardwick, 2007 Novel *sfi1* alleles uncover additional functions for Sfi1p in bipolar spindle assembly and function. Mol. Biol. Cell 18: 2047–2056.

Antoniacci, L. M., M. A. Kenna, P. Uetz, S. Fields, and R. V. Skibbens, 2004 The spindle pole body assembly component Mps3p/Nep98p functions in sister chromatid cohesion. J. Biol. Chem. 279: 49542–49550.

Araki, Y., C. K. Lau, H. Maekawa, S. L. Jaspersen, T. H. Giddings, Jr. *et al.*, 2006 The Saccharomyces cerevisiae spindle pole body (SPB) component Nbp1p is required for SPB membrane insertion and interacts with the integral membrane proteins Ndc1p and Mps2p. Mol. Biol. Cell 17: 1959–1970.

Ast, T., and M. Schuldiner, 2013 All roads lead to Rome (but some may be harder to travel): SRP-independent translocation into the endoplasmic reticulum. Crit. Rev. Biochem. Mol. Biol. 48: 273–288.

Baum, P., C. Furlong, and B. Byers, 1986 Yeast gene required for spindle pole body duplication: homology of its product with Ca^{2+}-binding proteins. Proc. Natl. Acad. Sci. USA 83: 5512–5516.

Bevington, P., and D. K. Robinson, 2003 *Data Reduction and Error Analysis for the Physical Sciences*, pp. 194–218. McGraw-Hill, New York.

Biggins, S., and M. D. Rose, 1994 Direct interaction between yeast spindle pole body components: Kar1p is required for Cdc31p localization to the spindle pole body. J. Cell Biol. 125: 843–852.

Brizzio, V., W. Khalfan, D. Huddler, C. T. Beh, S. S. Andersen *et al.*, 1999 Genetic interactions between KAR7/SEC71, KAR8/JEM1, KAR5, and KAR2 during nuclear fusion in Saccharomyces cerevisiae. Mol. Biol. Cell 10: 609–626.

Bullitt, E., M. P. Rout, J. V. Kilmartin, and C. W. Akey, 1997 The yeast spindle pole body is assembled around a central crystal of Spc42p. Cell 89: 1077–1086.

Bupp, J. M., A. E. Martin, E. S. Stensrud, and S. L. Jaspersen, 2007 Telomere anchoring at the nuclear periphery requires the budding yeast Sad1-UNC-84 domain protein Mps3. J. Cell Biol. 179: 845–854.

Burns, S., J. S. Avena, J. R. Unruh, Z. Yu, S. E. Smith *et al.*, 2015 Structured illumination with particle averaging reveals novel roles for yeast centrosome components during duplication. eLife .10.7554/eLife.08586

Byers, B., and L. Goetsch, 1974 Duplication of spindle plaques and integration of the yeast cell cycle. Cold Spring Harb. Symp. Quant. Biol. 38: 123–131.

Byers, B., and L. Goetsch, 1975 Behavior of spindles and spindle plaques in the cell cycle and conjugation of *Saccharomyces cerevisiae*. J. Bacteriol. 124: 511–523.

Casey, A. K., T. R. Dawson, J. Chen, J. M. Friederichs, S. L. Jaspersen *et al.*, 2012 Integrity and function of the *Saccharomyces cerevisiae* spindle pole body depends on connections between the membrane proteins Ndc1, Rtn1, and Yop1. Genetics 192: 441–455.

Chen, J., C. J. Smoyer, B. D. Slaughter, J. R. Unruh, and S. L. Jaspersen, 2014 The SUN protein Mps3 controls Ndc1 distribution and function on the nuclear membrane. J. Cell Biol. 204: 523–539.

Chial, H. J., M. P. Rout, T. H. Giddings, and M. Winey, 1998 *Saccharomyces cerevisiae* Ndc1p is a shared component of nuclear pore complexes and spindle pole bodies. J. Cell Biol. 143: 1789–1800.

Chook, Y. M., and G. Blobel, 2001 Karyopherins and nuclear import. Curr. Opin. Struct. Biol. 11: 703–715.

Conrad, M. N., C. Y. Lee, J. L. Wilkerson, and M. E. Dresser, 2007 *MPS3* mediates meiotic bouquet formation in Saccharomyces cerevisiae. Proc. Natl. Acad. Sci. USA 104: 8863–8868.

Conrad, M. N., C. Y. Lee, G. Chao, M. Shinohara, H. Kosaka *et al.*, 2008 Rapid telomere movement in meiotic prophase

is promoted by *NDJ1*, *MPS3*, and *CSM4* and is modulated by recombination. Cell 133: 1175–1187.
Copic, A., C. F. Latham, M. A. Horlbeck, J. G. D'Arcangelo, and E. A. Miller, 2012 ER cargo properties specify a requirement for COPII coat rigidity mediated by Sec13p. Science 335: 1359–1362.
Dawson, T. R., M. D. Lazarus, M. W. Hetzer, and S. R. Wente, 2009 ER membrane-bending proteins are necessary for de novo nuclear pore formation. J. Cell Biol. 184: 659–675.
Doucet, C. M., J. A. Talamas, and M. W. Hetzer, 2010 Cell cycle-dependent differences in nuclear pore complex assembly in metazoa. Cell 141: 1030–1041.
Drin, G., and B. Antonny, 2010 Amphipathic helices and membrane curvature. FEBS Lett. 584: 1840–1847.
Duden, R., M. Hosobuchi, S. Hamamoto, M. Winey, B. Byers *et al.*, 1994 Yeast β- and β′-coat proteins (COP). J. Biol. Chem. 269: 24486–24495.
Fang, H., and N. Green, 1994 Nonlethal sec71–1 and sec72–1 mutations eliminate proteins associated with the Sec63p-BiP complex from S. cerevisiae. Mol. Biol. Cell 5: 933–942.
Feldheim, D., K. Yoshimura, A. Admon, and R. Schekman, 1993 Structural and functional characterization of Sec66p, a new subunit of the polypeptide translocation apparatus in the yeast endoplasmic reticulum. Mol. Biol. Cell 4: 931–939.
Friederichs, J. M., S. Ghosh, C. J. Smoyer, S. McCroskey, B. D. Miller *et al.*, 2011 The SUN protein Mps3 is required for spindle pole body insertion into the nuclear membrane and nuclear envelope homeostasis. PLoS Genet. 7: e1002365.
Galy, V., J. C. Olivo-Marin, H. Scherthan, V. Doye, N. Rascalou *et al.*, 2000 Nuclear pore complexes in the organization of silent telomeric chromatin. Nature 403: 108–112.
Ghosh, S., J. M. Gardner, C. J. Smoyer, J. M. Friederichs, J. R. Unruh *et al.*, 2012 Acetylation of the SUN protein Mps3 by Eco1 regulates its function in nuclear organization. Mol. Biol. Cell 23: 2546–2559.
Green, N., H. Fang, and P. Walter, 1992 Mutants in three novel complementation groups inhibit membrane protein insertion into and soluble protein translocation across the endoplasmic reticulum membrane of Saccharomyces cerevisiae. J. Cell Biol. 116: 597–604.
Greenland, K. B., H. Ding, M. Costanzo, C. Boone, and T. N. Davis, 2010 Identification of *Saccharomyces cerevisiae* spindle pole body remodeling factors. PLoS One 5: e15426.
Hediger, F., F. R. Neumann, G. Van Houwe, K. Dubrana, and S. M. Gasser, 2002 Live imaging of telomeres: yKu and Sir proteins define redundant telomere-anchoring pathways in yeast. Curr. Biol. 12: 2076–2089.
Hetzer, M. W., and S. R. Wente, 2009 Border control at the nucleus: biogenesis and organization of the nuclear membrane and pore complexes. Dev. Cell 17: 606–616.
Jan, C. H., C. C. Williams, and J. S. Weissman, 2014 Principles of ER cotranslational translocation revealed by proximity-specific ribosome profiling. Science 346: 1257521.
Jaspersen, S. L., and S. Ghosh, 2012 Nuclear envelope insertion of spindle pole bodies and nuclear pore complexes. Nucleus 3: 226–236.
Jaspersen, S. L., and M. Winey, 2004 The budding yeast spindle pole body: structure, duplication, and function. Annu. Rev. Cell Dev. Biol. 20: 1–28.
Jaspersen, S. L., T. H. Giddings, Jr., and M. Winey, 2002 Mps3p is a novel component of the yeast spindle pole body that interacts with the yeast centrin homologue Cdc31p. J. Cell Biol. 159: 945–956.
Jaspersen, S. L., A. E. Martin, G. Glazko, T. H. Giddings, Jr., G. Morgan *et al.*, 2006 The Sad1-UNC-84 homology domain in Mps3 interacts with Mps2 to connect the spindle pole body with the nuclear envelope. J. Cell Biol. 174: 665–675.
Jones, G. M., J. Stalker, S. Humphray, A. West, T. Cox *et al.*, 2008 A systematic library for comprehensive overexpression screens in Saccharomyces cerevisiae. Nat. Methods 5: 239–241.
Jorgensen, P., N. P. Edgington, B. L. Schneider, I. Rupes, M. Tyers *et al.*, 2007 The size of the nucleus increases as yeast cells grow. Mol. Biol. Cell 18: 3523–3532.
Kilmartin, J. V., 2003 Sfi1p has conserved centrin-binding sites and an essential function in budding yeast spindle pole body duplication. J. Cell Biol. 162: 1211–1221.
Kilmartin, J. V., 2014 Lessons from yeast: the spindle pole body and the centrosome. Philos. Trans. R. Soc. Lond. B Biol. Sci. 369: pii: 20130456.
Kim, S. J., J. Fernandez-Martinez, P. Sampathkumar, A. Martel, T. Matsui *et al.*, 2014 Integrative structure-function mapping of the nucleoporin Nup133 suggests a conserved mechanism for membrane anchoring of the nuclear pore complex. Mol. Cell. Proteomics 13: 2911–2926.
Koszul, R., K. P. Kim, M. Prentiss, N. Kleckner, and S. Kameoka, 2008 Meiotic chromosomes move by linkage to dynamic actin cables with transduction of force through the nuclear envelope. Cell 133: 1188–1201.
Kupke, T., L. Di Cecco, H. M. Muller, A. Neuner, F. Adolf *et al.*, 2011 Targeting of Nbp1 to the inner nuclear membrane is essential for spindle pole body duplication. EMBO J. 30: 3337–3352.
Kurihara, T., and P. Silver, 1993 Suppression of a sec63 mutation identifies a novel component of the yeast endoplasmic reticulum translocation apparatus. Mol. Biol. Cell 4: 919–930.
Lau, C. K., V. A. Delmar, and D. J. Forbes, 2006 Topology of yeast Ndc1p: predictions for the human NDC1/NET3 homologue. Anat. Rec. A Discov. Mol. Cell. Evol. Biol. 288: 681–694.
Lee, C. Y., M. N. Conrad, and M. E. Dresser, 2012 Meiotic chromosome pairing is promoted by telomere-led chromosome movements independent of bouquet formation. PLoS Genet. 8: e1002730.
Lee, D. C., and J. D. Aitchison, 1999 Kap104p-mediated nuclear import. Nuclear localization signals in mRNA-binding proteins and the role of Ran and Rna. J. Biol. Chem. 274: 29031–29037.
Li, P., Y. Shao, H. Jin, and H. G. Yu, 2015 Ndj1, a telomere-associated protein, regulates centrosome separation in budding yeast meiosis. J. Cell Biol. 209: 247–259.
Longtine, M. S., A. McKenzie, 3rd, D. J. Demarini, N. G. Shah, A. Wach *et al.*, 1998 Additional modules for versatile and economical PCR-based gene deletion and modification in Saccharomyces cerevisiae. Yeast 14: 953–961.
Madrid, A. S., J. Mancuso, W. Z. Cande, and K. Weis, 2006 The role of the integral membrane nucleoporins Ndc1p and Pom152p in nuclear pore complex assembly and function. J. Cell Biol. 173: 361–371.
Mandon, E. C., S. F. Trueman, and R. Gilmore, 2013 Protein translocation across the rough endoplasmic reticulum. Cold Spring Harb. Perspect. Biol. 5: pii: a013342.
Miao, M., K. J. Ryan, and S. R. Wente, 2006 The integral membrane protein Pom34p functionally links nucleoporin subcomplexes. Genetics 172: 1441–1457.
Moens, P. B., and E. Rapport, 1971 Spindles, spindle plaques, and meiosis in the yeast Saccharomyces cerevisiae (Hansen). J. Cell Biol. 50: 344–361.
Muller, E. G., B. E. Snydsman, I. Novik, D. W. Hailey, D. R. Gestaut *et al.*, 2005 The organization of the core proteins of the yeast spindle pole body. Mol. Biol. Cell 16: 3341–3352.
Munoz-Centeno, M. C., S. McBratney, A. Monterrosa, B. Byers, C. Mann *et al.*, 1999 Saccharomyces cerevisiae MPS2 encodes a membrane protein localized at the spindle pole body and the nuclear envelope. Mol. Biol. Cell 10: 2393–2406.

Nishikawa, S., Y. Terazawa, T. Nakayama, A. Hirata, T. Makio *et al.*, 2003 Nep98p is a component of the yeast spindle pole body and essential for nuclear division and fusion. J. Biol. Chem. 278: 9938–9943.

O'Toole, E. T., M. Winey, and J. R. McIntosh, 1999 High-voltage electron tomography of spindle pole bodies and early mitotic spindles in the yeast Saccharomyces cerevisiae. Mol. Biol. Cell 10: 2017–2031.

Onischenko, E., L. H. Stanton, A. S. Madrid, T. Kieselbach, and K. Weis, 2009 Role of the Ndc1 interaction network in yeast nuclear pore complex assembly and maintenance. J. Cell Biol. 185: 475–491.

Park, E., and T. A. Rapoport, 2012 Mechanisms of Sec61/SecY-mediated protein translocation across membranes. Annu. Rev. Biophys. 41: 21–40.

Rogers, J. V., and M. D. Rose, 2014 Kar5p is required for multiple functions in both inner and outer nuclear envelope fusion in Saccharomyces cerevisiae. G3 5: 111–121.

Rossanese, O. W., C. A. Reinke, B. J. Bevis, A. T. Hammond, I. B. Sears *et al.*, 2001 A role for actin, Cdc1p, and Myo2p in the inheritance of late Golgi elements in Saccharomyces cerevisiae. J. Cell Biol. 153: 47–62.

Rout, M. P., J. D. Aitchison, A. Suprapto, K. Hjertaas, Y. Zhao *et al.*, 2000 The yeast nuclear pore complex: composition, architecture, and transport mechanism. J. Cell Biol. 148: 635–651.

Schober, H., H. Ferreira, V. Kalck, L. R. Gehlen, and S. M. Gasser, 2009 Yeast telomerase and the SUN domain protein Mps3 anchor telomeres and repress subtelomeric recombination. Genes Dev. 23: 928–938.

Schramm, C., S. Elliott, A. Shevchenko, and E. Schiebel, 2000 The Bbp1p-Mps2p complex connects the SPB to the nuclear envelope and is essential for SPB duplication. EMBO J. 19: 421–433.

Sezen, B., M. Seedorf, and E. Schiebel, 2009 The SESA network links duplication of the yeast centrosome with the protein translation machinery. Genes Dev. 23: 1559–1570.

Shao, S., and R. S. Hegde, 2011 Membrane protein insertion at the endoplasmic reticulum. Annu. Rev. Cell Dev. Biol. 27: 25–56.

Sheff, M. A., and K. S. Thorn, 2004 Optimized cassettes for fluorescent protein tagging in *Saccharomyces cerevisiae*. Yeast 21: 661–670.

Spang, A., I. Courtney, U. Fackler, M. Matzner, and E. Schiebel, 1993 The calcium-binding protein cell division cycle 31 of Saccharomyces cerevisiae is a component of the half bridge of the spindle pole body. J. Cell Biol. 123: 405–416.

Spang, A., I. Courtney, K. Grein, M. Matzner, and E. Schiebel, 1995 The Cdc31p-binding protein Kar1p is a component of the half bridge of the yeast spindle pole body. J. Cell Biol. 128: 863–877.

Spencer, F., S. L. Gerring, C. Connelly, and P. Hieter, 1990 Mitotic chromosome transmission fidelity mutants in Saccharomyces cerevisiae. Genetics 124: 237–249.

Stade, K., C. S. Ford, C. Guthrie, and K. Weis, 1997 Exportin 1 (Crm1p) is an essential nuclear export factor. Cell 90: 1041–1050.

Straight, A. F., A. S. Belmont, C. C. Robinett, and A. W. Murray, 1996 GFP tagging of budding yeast chromosomes reveals that protein-protein interactions can mediate sister chromatid cohesion. Curr. Biol. 6: 1599–1608.

Strambio-De-Castillia, C., M. Niepel, and M. P. Rout, 2010 The nuclear pore complex: bridging nuclear transport and gene regulation. Nat. Rev. Mol. Cell Biol. 11: 490–501.

Tcheperegine, S. E., M. Marelli, and R. W. Wozniak, 1999 Topology and functional domains of the yeast pore membrane protein Pom152p. J. Biol. Chem. 274: 5252–5258.

Therizols, P., C. Fairhead, G. G. Cabal, A. Genovesio, J. C. Olivo-Marin *et al.*, 2006 Telomere tethering at the nuclear periphery is essential for efficient DNA double strand break repair in subtelomeric region. J. Cell Biol. 172: 189–199.

Tong, A. H., and C. Boone, 2006 Synthetic genetic array analysis in *Saccharomyces cerevisiae*. Methods Mol. Biol. 313: 171–192.

Vallen, E. A., M. A. Hiller, T. Y. Scherson, and M. D. Rose, 1992 Separate domains of KAR1 mediate distinct functions in mitosis and nuclear fusion. J. Cell Biol. 117: 1277–1287.

Vallen, E. A., W. Ho, M. Winey, and M. D. Rose, 1994 Genetic interactions between CDC31 and KAR1, two genes required for duplication of the microtubule organizing center in Saccharomyces cerevisiae. Genetics 137: 407–422.

Van de Vosse, D. W., Y. Wan, D. L. Lapetina, W. M. Chen, J. H. Chiang *et al.*, 2013 A role for the nucleoporin Nup170p in chromatin structure and gene silencing. Cell 152: 969–983.

West, R. R., E. V. Vaisberg, R. Ding, P. Nurse, and J. R. McIntosh, 1998 cut11(+): A gene required for cell cycle-dependent spindle pole body anchoring in the nuclear envelope and bipolar spindle formation in Schizosaccharomyces pombe. Mol. Biol. Cell 9: 2839–2855.

Wigge, P. A., O. N. Jensen, S. Holmes, S. Soues, M. Mann *et al.*, 1998 Analysis of the Saccharomyces spindle pole by matrix-assisted laser desorption/ionization (MALDI) mass spectrometry. J. Cell Biol. 141: 967–977.

Winey, M., and K. Bloom, 2012 Mitotic spindle form and function. Genetics 190: 1197–1224.

Winey, M., L. Goetsch, P. Baum, and B. Byers, 1991 MPS1 and MPS2: novel yeast genes defining distinct steps of spindle pole body duplication. J. Cell Biol. 114: 745–754.

Winey, M., M. A. Hoyt, C. Chan, L. Goetsch, D. Botstein *et al.*, 1993 NDC1: a nuclear periphery component required for yeast spindle pole body duplication. J. Cell Biol. 122: 743–751.

Witkin, K. L., J. M. Friederichs, O. Cohen-Fix, and S. L. Jaspersen, 2010 Changes in the nuclear envelope environment affect spindle pole body duplication in *Saccharomyces cerevisiae*. Genetics 186: 867–883.

Witkin, K. L., Y. Chong, S. Shao, M. T. Webster, S. Lahiri *et al.*, 2012 The budding yeast nuclear envelope adjacent to the nucleolus serves as a membrane sink during mitotic delay. Curr. Biol. 22: 1128–1133.

Wozniak, R. W., G. Blobel, and M. P. Rout, 1994 POM152 is an integral protein of the pore membrane domain of the yeast nuclear envelope. J. Cell Biol. 125: 31–42.

Yu, L., L. Pena Castillo, S. Mnaimneh, T. R. Hughes, and G. W. Brown, 2006 A survey of essential gene function in the yeast cell division cycle. Mol. Biol. Cell 17: 4736–4747.

Communicating editor: O. Cohen-Fix

GENETICS

Supporting Information
www.genetics.org/lookup/suppl/doi:10.1534/genetics.115.178012/-/DC1

Sec66-Dependent Regulation of Yeast Spindle-Pole Body Duplication Through Pom152

Santharam S. Katta, Jingjing Chen, Jennifer M. Gardner, Jennifer M. Friederichs, Sarah E. Smith, Madelaine Gogol, Jay R. Unruh, Brian D. Slaughter, and Sue L. Jaspersen

DOI: 10.1534/genetics.115.178012

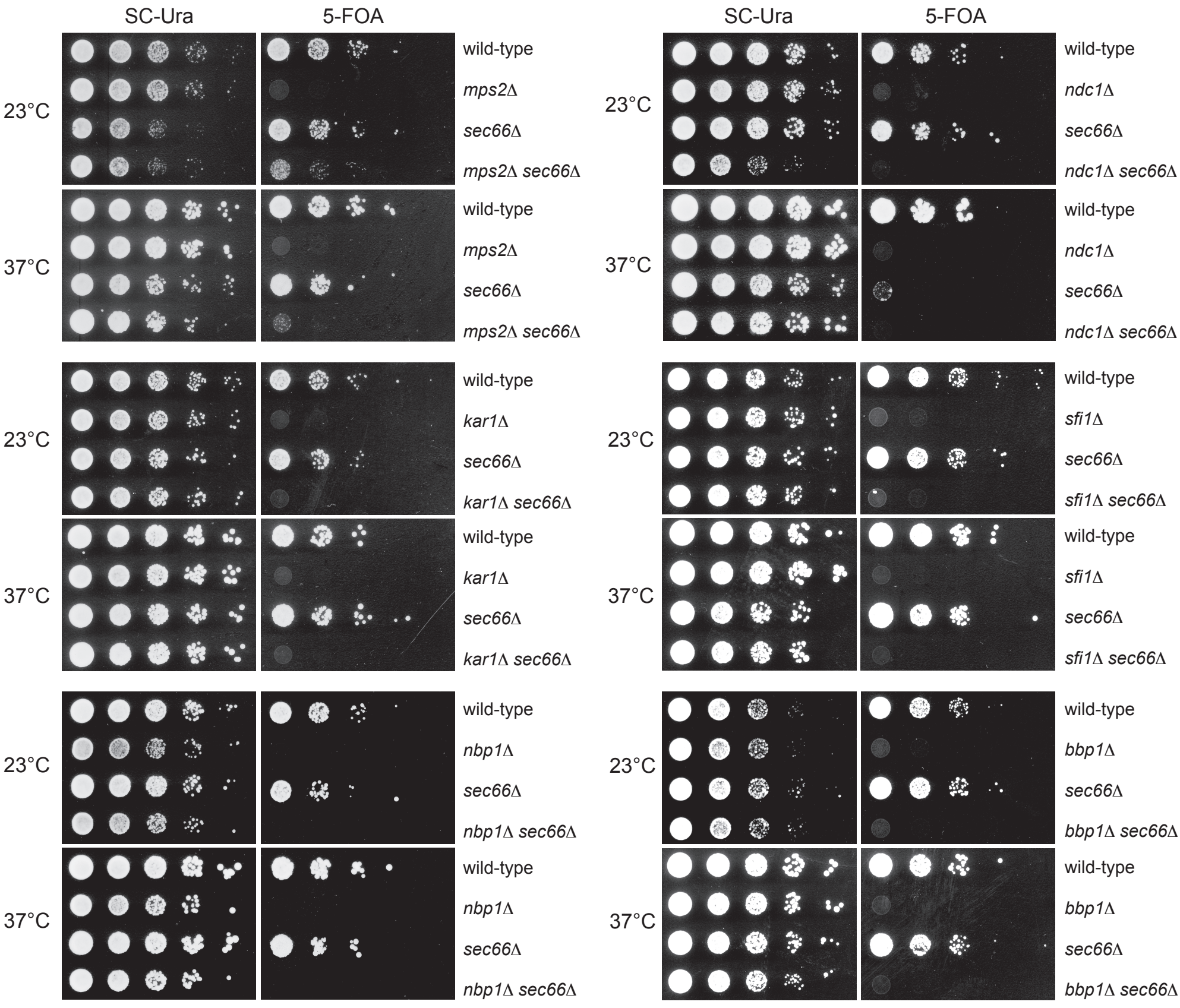

Figure S1. Deletion of *SEC66* partially bypasses the requirement for *MPS2* but not other SPB components.
In the W303 background, *sec66*Δ (SLJ6997) was crossed to *mps2*Δ *pURA3-MPS2* (SLJ5099), *kar1*Δ *pURA3-KAR1* (SLJ5102), *nbp1*Δ *pURA3-NBP1* (SLJ4282), *sfi1*Δ *pURA3-SFI1* (SLJ9449) and *bbp1*Δ *pURA3-BBP1* (SLJ9338) and *sec66*Δ (SLJ6968) to *ndc1*Δ *pURA3-NDC1* (SLJ6059). Cells were sporulated and tetrads dissected and analyzed. 10-fold serial dilutions of cells from a tetratype tetrad were spotted onto SC-Ura or 5-FOA and incubated at 23°C for 3 d or 37°C for 2 d.

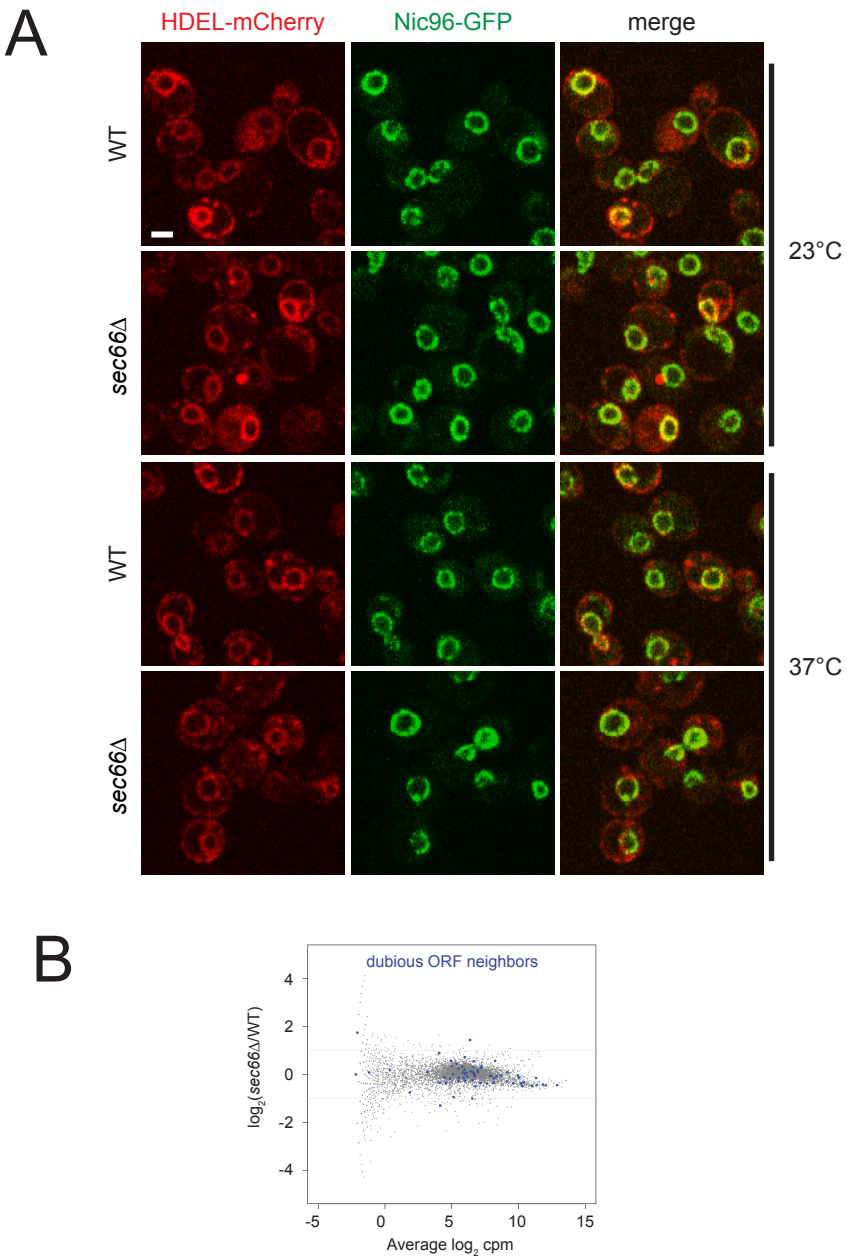

Figure S2. Expression of genes adjacent to dubious ORFs.
A. Wild-type and *sec66*Δ cells containing the ER marker HDEL-dsRed (red) and the NPC subunits Nic96-GFP (green) (SLJ10647 and SLJ10648) were grown at 23°C then half the culture was shifted to 37°C for 4 h prior to imaging. Bar, 2 µm. B. Genes in wild-type (SLJ173) versus *sec66*Δ (SLJ5281) cells are shown in the plot, with average counts on the x-axis and the change in expression on the y-axis. Dashed lines at -1 and 1 indicate a 2-fold change in expression. The position of genes upstream and downstream of the dubious ORFs is highlighted.

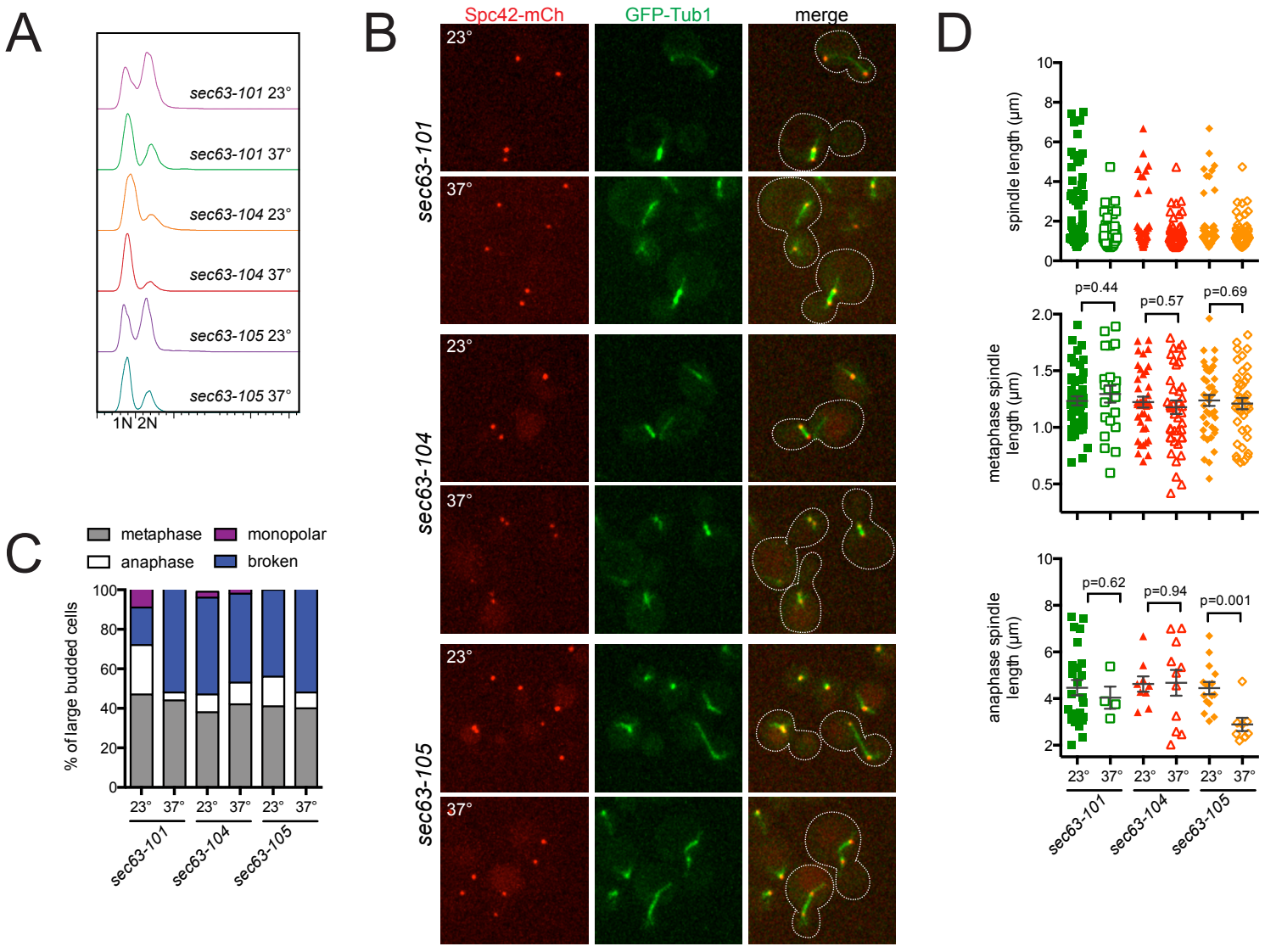

Figure S3. Spindle defects in *sec63* mutants.
sec63-101 (SLJ10773), *sec63-104* (SLJ10774) and *sec63-105* (SLJ10807) cells containing Spc42-mCherry (red) and GFP-Tub1 (green) to visualize the SPB and microtubules, respectively, were grown to log phase at 23°C then half the culture was shifted to 37°C for 4 h. A. Flow cytometric analysis of DNA content. B. Examples images of large budded cells are shown, with dashed lines drawn based on brightfield image. Bar, 2 µm. C. In at least 100 large budded cells, spindle morphology was analyzed. Monopolar spindles (large budded cells containing a single SPB or containing two SPBs, only one of which nucleates nuclear microtubules) and broken spindles (large budded cells with two separated SPBs that contain non-overlapping arrays of nuclear microtubules) were observed. The percentage of metaphase and anaphase spindles was determined using the natural gap in length that occurred at 2 µm in all strains. D. Average spindle length is shown by the long bar; shorter bars show SEM. p values calculated using Student's t-test are listed. In addition to broken and monopolar spindles, we observed cells that contained bipolar spindles within the daughter cell (see *sec63-104* at both 23°C and 37°C).

Table S1. Suppressors of *mps3*Δ.

ORF name	gene	alias	*mps3*Δ W303*	function
YBR171W	*SEC66*	*HSS1, SEC71*	yes	Non-essential subunit of Sec63 complex; with Sec61 complex, Kar2p/BiP and Lhs1p forms a channel competent for SRP-dependent and post-translational SRP-independent protein targeting and import into the ER
YBR196C-A			no	Putative protein of unknown function
YCR107W	*AAD3*		no	Putative aryl-alcohol dehydrogenase; mutational analysis has not yet revealed a physiological role
YDR014W	*RAD61*	*WPL1*	nd	Subunit of a complex that inhibits sister chromatid cohesion
YDR025W	*RPS11A*		nd	Protein component of the small (40S) ribosomal subunit
YDR072C	*IPT1*	*MIC,2 KTI6, SYR4*	no	Inositolphosphotransferase; involved in synthesis of mannose-(inositol-P)2-ceramide (M(IP)2C), the most abundant sphingolipid
YDR138W	*HPR1*	*TRF1*	no	Subunit of THO/TREX complex to couple transcription elongation with mitotic recombination and with mRNA metabolism and export; regulates lifespan; involved in telomere maintenance

YDR273W	*DON1*		nd	Meiosis-specific component of the spindle pole body; part of the leading edge protein (LEP) coat, forms a ring-like structure at the leading edge of the prospore membrane during meiosis II;
YGL136C	*MRM2*		no	Mitochondrial 2' O-ribose methyltransferase; required for methylation of U(2791) in 21S rRNA
YGL151W	*NUT1*	*SSX, MED5*	no	Component of the RNA polymerase II mediator complex
YGL206C	*CHC1*	*SWA5*	no	Clathrin heavy chain; subunit of the major coat protein involved in intracellular protein transport and endocytosis
YGL261C	*PAU11*		no	Putative protein of unknown function; member of the seripauperin multigene family encoded mainly in subtelomeric regions
YGR143W	*SKN1*		no	Protein involved in sphingolipid biosynthesis
YLR018C	*POM34*		yes	Subunit of the transmembrane ring of the nuclear pore complex (NPC); contributes to nucleocytoplasmic transport, NPC biogenesis and spindle pole body duplication
YLR338W	*OPI9*	*(VRP1)*	nd	Dubious open reading frame; paritally overlaps with *VRP1*, a proline-rich actin-associated protein; involved in actin nucleation, endocytosis and cytokinesis

YLR368W	*MDM30*	*DSG1*	no	F-box component of an SCF ubiquitin protein ligase complex; associates with and is required for Fzo1p ubiquitination and for mitochondria fusion; stimulates nuclear export of specific mRNAs
YMR129W	*POM152*		yes	Glycoprotein subunit of transmembrane ring of nuclear pore complex; contributes to nucleocytoplasmic transport, nuclear pore complex (NPC) biogenesis and spindle pole body duplication
YOR239W	*ABP140*	*YOR240W, TRM140*	no	AdoMet-dependent tRNA methyltransferase and actin binding protein
YPL090C	*RPS6A*		nd	Protein component of the small (40S) ribosomal subunit
YPR043W	*RPL43A*		nd	Ribosomal 60S subunit protein L43A
YPR045C	*THP3*	*MNI2*	no	Protein that may have a role in transcription elongation; forms a complex with Csn12p that is recruited to transcribed genes
YPR092W		(NVJ2)	no	Dubious open reading frame that overlaps with NVJ2, a lipid-binding ER protein, enriched at nucleus-vacuolar junctions (NVJ); may be involved in sterol metabolism or signaling at the NVJ

* deletions were remade in a W303 strain containing *mps3*Δ p*URA3-MPS3* then tested for their ability to grow on 5-FOA; yes, growth on 5-FOA; no, no growth on 5-FOA; nd, not determined

Table S2. Chromosome XIII hits.

MPS3	*MPS2*	*NBP1*	*KAR1*	*CDC31*	*SFI1*	Combined	Gene
	■					YML048W	*GSF2*
■	■		■	■	■	YML051W	*GAL80*
■	■		■	■	■	YML061C	*PIF1*
					■	YML062C	*MFT1*
■	■		■	■	■	YML063W	*RPS1B*
■	■		■	■		YML078W	*CPR3*
■	■		■	■	■	YML079W	
■	■		■	■	■	YML080W	*DUS1*
■	■		■	■		YML081W	*TDA9*
■	■		■	■		YML082W	
■			■	■		YML083C	
■	■		■	■	■	YML084W	
	■		■	■	■	YML086C	*ALO1*
■	■		■	■	■	YML087C	*AIM33*
■	■		■	■		YML088W	*UFO1*
■	■		■	■		YML089C	

Black boxes show hits from the indicated region along chromosome XIII that came up as hits in the SPB bypass suppressor screen.

Table S3. Sec66-dependent transcripts.

ORF	Gene Name	*sec66*Δ vs WT log2fc	*sec66*Δ vs WT pval
YBR171W	*SEC66*	-10.2880004	0
YLR062C	*BUD28*	-5.486434555	0.000156377
YDR209C	*YDR209C*	-4.295857687	0.017130425
tF(GAA)M	*tF(GAA)M*	-4.066645471	0.034235269
YHR079C-A	*SAE3*	-4.054847897	0.033219158
YLR076C	*YLR076C*	-3.642764627	0.000713944
YGR190C	*YGR190C*	-2.781392901	0.042814708
YHR056W-A	*YHR056W-A*	-2.757566482	0.002351011
YNL194C	*YNL194C*	-2.600037779	1.45E-08
YLL044W	*YLL044W*	-2.394228307	0.001732815
YJL188C	*BUD19*	-2.381327712	1.08E-05
YNR034W-A	*YNR034W-A*	-2.353961449	6.29E-19
YPR050C	*YPR050C*	-2.277526846	0.005605854
YPL250W-A	*YPL250W-A*	-2.237565321	0.000749816
YOR178C	*GAC1*	-2.147570558	2.87E-09
YER078W-A	*YER078W-A*	-2.132870744	0.016353188
YCR021C	*HSP30*	-2.107740157	0.002656172
YBR054W	*YRO2*	-2.050641111	2.57E-09
YER067W	*RGI1*	-2.000876054	7.76E-10
YGL255W	*ZRT1*	-1.99782713	1.05E-29
YNL174W	*YNL174W*	-1.879993942	0.025228476
YGL102C	*YGL102C*	-1.847132559	0.000174266
YBR093C	*PHO5*	-1.842011975	1.54E-25
YMR245W	*YMR245W*	-1.840916334	0.009112187
YAL059C-A	*YAL059C-A*	-1.832830554	0.015773239
YPR123C	*YPR123C*	-1.821792986	0.017209026
YER150W	*SPI1*	-1.73567611	0.000148842
YFR036W-A	*YFR036W-A*	-1.707286044	0.03669005
YMR122C	*YMR122C*	-1.621641101	0.04078201
YPR142C	*YPR142C*	-1.615796291	0.003216244
YLR255C	*YLR255C*	-1.611382332	0.039098568
YAL037C-B	*YAL037C-B*	-1.6092561	0.004041517
YGR052W	*FMP48*	-1.588796836	1.28E-13
YEL053W-A	*YEL053W-A*	-1.581634522	0.033508252
YBL049W	*MOH1*	-1.579161933	6.56E-07
YGL123C-A	*YGL123C-A*	-1.56179132	0.001303258
YGR088W	*CTT1*	-1.55400821	8.30E-11
YOR393W	*ERR1*	-1.540342252	0.012763129
YDR171W	*HSP42*	-1.513674929	0.000187228
YMR085W	*YMR085W*	-1.503429012	7.47E-05
YMR084W	*YMR084W*	-1.503326472	0.001949641
tK(UUU)P	*tK(UUU)P*	-1.473418834	0.011418737
YPR160W-A	*YPR160W-A*	-1.4229929	0.005901096
YHR087W	*RTC3*	-1.418151914	1.10E-06
YOR053W	*YOR053W*	-1.373040332	0.019455409
YEL034C-A	*YEL034C-A*	-1.362287935	0.017523617
YAR071W	*PHO11*	-1.360624145	9.05E-19
YHR215W	*PHO12*	-1.357642361	8.35E-20
YPL187W	*MF(ALPHA)1*	-1.34276221	0.032556093

YGR138C	*TPO2*	-1.337626195	0.000922046
YGR160W	*YGR160W*	-1.322036041	0.023910501
YNR014W	*YNR014W*	-1.306601308	6.94E-05
YPL250C	*ICY2*	-1.303993147	2.65E-10
YOR273C	*TPO4*	-1.303292941	0.000736433
YGL096W	*TOS8*	-1.257521507	0.000187126
YPR157W	*TDA6*	-1.255323373	0.000194205
YML100W	*TSL1*	-1.25403863	1.64E-13
YPL014W	*YPL014W*	-1.24223574	0.001187976
YHR139C	*SPS100*	-1.238293895	0.000750221
YDR119W-A	*YDR119W-A*	-1.237340604	0.000338856
YFR015C	*GSY1*	-1.225193838	2.22E-14
YOR161C	*PNS1*	-1.22261153	1.12E-16
YAL061W	*BDH2*	-1.219536416	0.000585374
YGR008C	*STF2*	-1.210841353	1.97E-05
YGR142W	*BTN2*	-1.201197112	5.23E-07
YFR032C	*RRT5*	-1.181384605	4.94E-05
YDL204W	*RTN2*	-1.161468728	4.72E-08
YIL113W	*SDP1*	-1.160566552	0.000685696
YMR081C	*ISF1*	-1.159914343	0.002268085
YOL084W	*PHM7*	-1.148366818	1.57E-05
YGR248W	*SOL4*	-1.142884304	6.74E-05
YJR018W	*YJR018W*	-1.14010918	0.019030745
YER188W	*YER188W*	-1.136101848	0.000137426
YJL142C	*IRC9*	-1.128668222	0.000663983
YOL153C	*YOL153C*	-1.117237892	0.003449447
YMR250W	*GAD1*	-1.114849554	7.22E-06
YGL179C	*TOS3*	-1.114362892	1.73E-05
YGR249W	*MGA1*	-1.109988486	0.010968082
YNL077W	*APJ1*	-1.091393604	2.18E-06
YBL048W	*RRT1*	-1.075328329	0.005400329
YDR074W	*TPS2*	-1.062314516	5.90E-07
snR190	*SNR190*	-1.060490288	0.024823597
YDL037C	*BSC1*	-1.05149752	1.29E-12
YPL165C	*SET6*	-1.050013994	6.23E-06
YEL011W	*GLC3*	-1.046633537	3.49E-09
YLL052C	*AQY2*	-1.032058588	4.03E-06
YDL039C	*PRM7*	-1.028681093	1.26E-12
YER053C	*PIC2*	-1.028188955	0.000502348
YHR216W	*IMD2*	-1.023757369	2.27E-10
YLR161W	*YLR161W*	-1.011504658	0.046144344
YJL141C	*YAK1*	-1.009501865	6.57E-05
YMR244W	*YMR244W*	-1.001061547	0.020577729
YEL065W	*SIT1*	1.039044351	4.60E-11
YJR079W	*YJR079W*	1.054224459	0.023831712
YKL065W-A	*YKL065W-A*	1.083089191	0.006233341
YLR109W	*AHP1*	1.085865436	2.77E-15
YOR338W	*YOR338W*	1.096599904	7.80E-13
YDR216W	*ADR1*	1.152002753	1.86E-05
YFR052C-A	*YFR052C-A*	1.154190348	0.000856472
YDR379C-A	*YDR379C-A*	1.160552069	5.97E-08
YNL276C	*YNL276C*	1.163607333	0.007991201

YBL043W	*ECM13*	1.195707174	6.57E-08
YLL062C	*MHT1*	1.213716162	4.35E-11
YDR214W	*AHA1*	1.224462224	4.45E-17
YNL198C	*YNL198C*	1.230980296	0.001493988
YIL141W	*YIL141W*	1.234164358	5.90E-06
YAL067C	*SEO1*	1.239996885	3.85E-05
YGR109C	*CLB6*	1.265496689	0.001307086
YBR294W	*SUL1*	1.418032243	2.13E-06
YFR053C	*HXK1*	1.431347425	7.49E-07
YHR069C-A	*YHR069C-A*	1.448600162	0.008446839
YOL038C-A	*YOL038C-A*	1.530245849	0.000108017
YDL186W	*YDL186W*	1.533401345	0.022679933
snR62	*SNR62*	1.555935314	0.002834202
YLR438W	*CAR2*	1.636506697	3.81E-08
YEL045C	*YEL045C*	1.644600039	0.001665849
tY(GUA)F1	*SUP11*	4.113705585	0.033577853
YBR072C-A	*YBR072C-A*	4.1164138	0.033303304
Q0275	*COX3*	4.117769535	0.033552379

Table S4. Yeast Strains.

Strain	Relavant Genotype	Experiment
SLJ2602	*Mata his3::GFP-LACI-HIS3 NUP49-GFP-URA3 TELVIR-LACOR-lexAo-TRP1 ADE2-TG1-3*	Figure 1B-D
SLJ3081	*Mata mps3Δ::mps3Δ75-150-NATMX his3::GFP-LACI-HIS3 NUP49-GFP-URA3 TELVIR-LACOR-lexAo-TRP1 ADE2-TG1-3TRP1 ADE2-TG1*	Figure 1B-D
SLJ4333	*Mata pom152Δ::HYGMX his3::GFP-LACI-HIS3 NUP49-GFP-URA3 TELVIR-LACOR-lexAo-TRP1 ADE2-TG1-3*	Figure 1B-D
SLJ4330	*Mata pom152Δ::HYGMX mps3Δ::NATMX his3::GFP-LACI-HIS3 NUP49-GFP-URA3 TELVIR-LACOR-lexAo-TRP1 ADE2-TG1-3*	Figure 1B-D
SLJ1982	*Mata leu2::PDS1-18xmyc-LEU2 his3::GFP-LACI-HIS3 trp1::256x LACOR-TRP1*	Figure 1E-G
SLJ3131	*Mata mps3Δ::mps3Δ75-150-NATMX leu2::PDS1-18xmyc-LEU2 his3::GFP-LACI-HIS3 trp1::256x LACOR-TRP1*	Figure 1F-G
SLJ4328	*Matα pom152Δ::HYGMX leu2::PDS1-18xmyc-LEU2 his3::GFP-LACI-HIS3 trp1::256x LACOR-TRP1*	Figure 1F-G
SLJ4325	*Mata pom152Δ::HYGMX mps3Δ::NATMX leu2::PDS1-18xmyc-LEU2 his3::GFP-LACI-HIS3 trp1::256x LACOR-TRP1*	Figure 1F-G
SLJ2156	*Mata ade2-1 ura3 leu2 trp1-1 lys2-801 his3 CAN1 CFIII (CEN 3.L. YPH278) URA3-SUPII*	Figure 1H
SLJ4547	*Mata pom152Δ::HYGMX ade2-1 ura3 leu2 trp1-1 lys2-801 his3 CAN1 CFIII (CEN 3.L. YPH278) URA3-SUPII*	Figure 1H
SLJ4548	*Mata pom152Δ::HYGMX mps3Δ::NATMX ade2-1 ura3 leu2 trp1-1 lys2-801 his3 CAN1 CFIII (CEN 3.L. YPH278) URA3-SUPII*	Figure 1H
SLJ1888	*Matα mps3Δ::NATMX can1Δ::STE2pr-SpHIS5 his3ΔO ura3ΔO leu2ΔO met15ΔO lyp1Δ pURA3-MPS3*	Figure 2A, C, Table S1, S2
SLJ4779	*Matα kar1Δ::NATMX can1Δ::STE2pr-SpHIS5 his3ΔO ura3ΔO leu2ΔO met15ΔO lyp1Δ pURA3-KAR1*	Figure 2C, Table S2
SLJ4781	*Matα mps2Δ::NATMX can1Δ::STE2pr-SpHIS5 his3ΔO ura3ΔO leu2ΔO met15ΔO lyp1Δ pURA3-MPS2*	Figure 2C, Table S2
SLJ5872	*Matα nbp1Δ::NATMX can1Δ::STE2pr-SpHIS5 his3ΔO ura3ΔO leu2ΔO met15ΔO lyp1Δ pURA3-NBP1*	Figure 2C, Table S2
SLJ6357	*Matα cdc31Δ::NATMX can1Δ::STE2pr-SpHIS5 his3ΔO ura3ΔO leu2ΔO met15ΔO lyp1Δ pURA3-CDC31*	Figure 2C, Table S2
SLJ6358	*Matα sfi1Δ::NATMX can1Δ::STE2pr-SpHIS5 his3ΔO ura3ΔO leu2ΔO met15ΔO lyp1Δ pURA3-SFI1*	Figure 2C, Table S2
SLJ8666	*Mata pURA3-MPS3*	Figure 2D, 3B, 3D, 5D
SLJ8667	*Mata mps3Δ::NATMX pURA3-MPS3*	Figure 2D, 3B, 3D
SLJ9550	*Mata pom152Δ::HYGMX pURA3-MPS3*	Figure 2D
SLJ4738	*Mata mps3Δ::NATMX pom152Δ::HYGMX pURA3-MPS3*	Figure 2D

SLJ9309	*Mata pom34Δ::KANMX pURA3-MPS3*	Figure 2D
SLJ9310	*Mata mps3Δ::NATMX pom34Δ::KANMX pURA3-MPS3*	Figure 2D
SLJ8668	*Mata sec66Δ::KANMX pURA3-MPS3*	Figure 2D, 3B
SLJ8669	*Mata mps3Δ::NATMX sec66Δ::KANMX pURA3-MPS3*	Figure 2D, 3B, 5D
SLJ4807	*Matα pURA3-MPS2*	Figure 2E, 3B
SLJ4808	*Matα mps2Δ::KANMX pURA3-MPS2*	Figure 2E
SLJ4809	*Mata pom152Δ::HYGMX pURA3-MPS2*	Figure 2E
SLJ4810	*Mata mps2Δ::KANMX pom152Δ::HYGMX pURA3-MPS2*	Figure 2E
SLJ4811	*Matα mps3Δ::NATMX pom152Δ::HYGMX pURA3-MPS2*	Figure 2E
SLJ4812	*Mata mps2Δ::KANMX mps3Δ::NATMX pom152Δ::HYGMX pURA3-MPS2*	Figure 2E
SLJ8670	*Mata mps3Δ::NATMX sec66Δ::KANMX pom152Δ::HYGMX pURA3-MPS3*	Figure 3B
SLJ7687	*Mata mps2Δ::NATMX pURA3-MPS2*	Figure 3C, S1
SLJ7686	*Mata sec66Δ::KANMX pURA3-MPS2*	Figure 3C, S1
SLJ7688	*Mata sec66Δ::KANMX mps2Δ::NATMX pURA3-MPS2*	Figure 3C, S1
SLJ8677	*Mata mps2Δ::NATMX sec66Δ::KANMX pom152Δ::HYGMX pURA3-MPS2*	Figure 3C
SLJ9469	*Mata sec72Δ::KANMX pURA3-MPS3*	Figure 3D
SLJ9489	*Mata mps3Δ::NATMX sec72Δ::KANMX pURA3-MPS3*	Figure 3D
SLJ9792	*Mata sbh1Δ::KANMX pURA3-MPS3*	Figure 3D
SLJ9791	*Mata mps3Δ::NATMX sbh1Δ::KANMX pURA3-MPS3*	Figure 3D
SLJ7238	*Mata ssh1Δ::KANMX pURA3-MPS3*	Figure 3D
SLJ7637	*Mata mps3Δ::NATMX ssh1Δ::KANMX pURA3-MPS3*	Figure 3D
SLJ10508	*Mata SEC66-GFP-NATMX pLEU2-SPC42-mCherry-HIS3MX*	Figure 3E
SLJ10647	*Mata NIC96-GFP-HIS3MX trp1::HDEL-DsRed-TRP1 ADE2*	Figure 4A, S2A
SLJ10648	*Mata sec66Δ::KANMX NIC96-GFP-HIS3MX trp1::HDEL-DsRed-TRP1 ADE2*	Figure 4A, S2A
SLJ10649	*Mata NUP192-GFP-HIS3MX trp1::HDEL-DsRed-TRP1 ADE2*	Figure 4A, S2A
SLJ10650	*Mata sec66Δ::KANMX NUP192-GFP-HIS3MX trp1::HDEL-DsRed-TRP1 ADE2*	Figure 4A, S2A
SLJ7996	*Mata NDC1-mCherry-HYGMX 2μ-LEU2-rgNLS-mutNE*	Figure 4B-C
SLJ7997	*Mata NDC1-mCherry-HYGMX pLEU2-cNLS-GFP*	Figure 4B-C
SLJ7998	*Matα sec66Δ::KANMX NDC1-mCherry-HYGMX 2μ-LE*	Figure 4B-C
SLJ7999	*Matα sec66Δ::KANMX NDC1-mCherry-HYGMX pLEU2-cNLS-GFP*	Figure 4B-C
SLJ8000	*Mata mps3Δ::NATMX sec66Δ::KANMX NDC1-mCherr*	Figure 4B-C
SLJ8001	*Mata mps3Δ::NATMX sec66Δ::KANMX NDC1-mCherr*	Figure 4B-C
SLJ6834	*Mata SPC42-mCherry-HYGMX GFP-TUB1-NATMX*	Figure 4E-F
SLJ10759	*Mata sec66Δ::KANMX SPC42-mCherry-HYGMX GFP-TUB1-NATMX*	Figure 4E-F
SLJ10775	*Mata sec72Δ::KANMX SPC42-mCherry-HYGMX GFP-TUB1-NATMX*	Figure 4E-F
SLJ10773	*Mata sec63-101 SPC42-mCherry-HYGMX GFP-TUB1-NATMX*	Figure 4F, S3
SLJ10774	*Mata sec63-104 SPC42-mCherry-HYGMX GFP-TUB1-NATMX*	Figure 4F, S3
SLJ10807	*Mata sec63-105 SPC42-mCherry-HYGMX GFP-TUB1-NATMX*	Figure 4F, S3

SLJ173	*Matα bar1::hisG ura3-1 leu2-3,112 trp1-1 his3-11,15 ade2-1 can1-100 GAL+*	Figure 4D, Table S3
SLJ5281	*Matα bar1::hisG sec66Δ::KANMX bar1::hisG ura3-1 leu2-3,112 trp1-1 his3-11,15 ade2-1 can1-100 GAL+*	Figure 4D, Table S3
SLJ8167	*Mata/α POM152-YFP-HIS3MX/POM152-YFP-HIS3MX*	Figure 5A-C
SLJ8168	*Mata/α POM152-YFP-HIS3MX/POM152-YFP-HIS3MX sec66Δ::KANMX/sec66Δ::KANMX*	Figure 5A-C
SLJ8339	*Mata/α POM152-YFP-HIS3MX/POM152-YFP-HIS3MX sec66Δ::KANMX/sec66Δ::KANMX mps3Δ::NATMX/mps3Δ::NATMX*	Figure 5A-C
SLJ7824	*Mata/α POM34-YFP-HIS3MX/POM34-YFP-HIS3MX*	Figure 5A-C
SLJ7854	*Mata/α POM34-YFP-HIS3/POM34-YFP-HIS3 sec66Δ::KANMX/sec66Δ::KANMX*	Figure 5A-C
SLJ7895	*Mata/α POM34-YFP-HIS3MX/POM34-YFP-HIS3MX sec66Δ::KANMX/sec66Δ::KANMX mps3Δ::NATMX/mps3Δ::NATMX*	Figure 5A-C
SLJ7936	*Mata/α NDC1-GFP-HYGMX/NDC1::NDC1-GFP-HYGMX*	Figure 5C
SLJ7937	*Mata/α NDC1-GFP-HYGMX/NDC1-GFP-HYGMX sec66Δ::KANMX/sec66Δ::KANMX*	Figure 5C
SLJ7938	*Mata/α NDC1-GFP-HYGMX/NDC1-GFP-HYGMX mps3Δ::NATMX/mps3Δ::NATMX sec66Δ::KANMX/sec66Δ::KANMX*	Figure 5C
SLJ9253	*Mata leu2::GAL-POM152-LEU2*	Figure 5E
SLJ9259	*Mata leu2::GAL-POM152-LEU2 sec66Δ::KANMX*	Figure 5E
SLJ9262	*Mata leu2::GAL-POM152-LEU2 mps3Δ::NATMX sec66Δ::KANMX*	Figure 5E
SLJ9356	*Matα NBP1-mTurq-URA NDC1-YFP-HIS ADE2 LYS2*	Figure 6A-D
SLJ9357	*Matα sec66Δ::KANMX NBP1-mTurq-URA NDC1-YFP-HIS ADE2 LYS2*	Figure 6A-D
SLJ10808	*Mata mps3Δ::NATMX sec66Δ::KANMX NBP1-mTurq-HYGMX NDC1-YFP-HIS ADE2 pURA3-MPS3*	Figure 6A-D
SLJ8173	*Mata/α SPC42-mTurquoise2-URA3MX/SPC42-mTurquoise2-URA3MX CNM67-YFP-HIS3MX/CNM67-YFP-HIS3MX*	Figure 6D
SLJ9012	*Matα YFP-SPC110-mTurquoise2-URAMX*	Figure 6D
SLJ5027	*Mata/α pURA3-MPS3*	Figure 7A
SLJ10344	*Mata/α mps3Δ::KANMX/mps3Δ::NATMX pURA3-MPS3*	Figure 7A
SLJ9856	*Mata/α POM152/pom152Δ::HYGMX mps3Δ::NATMX/mps3Δ::NATMX pURA3-MPS3*	Figure 7A
SLJ5023	*Mata/α pom152Δ::HYGMX/pom152Δ::HYGMX mps3Δ::NATMX/mps3Δ::NATMX pURA3-MPS3*	Figure 7A
SLJ10345	*Mata/α POM34/pom34Δ::KANMX mps3Δ::NATMX/mps3Δ::NATMX pURA3-MPS3*	Figure 7A
SLJ10346	*Mata/α pom34Δ::HYGMX/pom34Δ::KANMX mps3Δ::NATMX/mps3Δ::NATMX pURA3-MPS4*	Figure 7A
SLJ6170	*Matα ndc1Δ::KANMX::ndc1-A290E-TRP1-KANMX pU*	Figure 7B
SLJ6179	*Matα pom152Δ::NATMX ndc1Δ::KANMX::ndc1-A290E*	Figure 7B
SLJ6177	*Matα ndc1Δ::KANMX::ndc1-L562S-TRP1-KANMX pU*	Figure 7B
SLJ6180	*Matα pom152Δ::NATMX ndc1Δ::KANMX::ndc1-L562S*	Figure 7B
SLJ6166	*Matα ndc1Δ::KANMX::NDC1-TRP1-KANMX pURA3-N*	Figure 7B
SLJ6178	*Matα pom152Δ::NATMX ndc1Δ::KANMX::NDC1-TRP1*	Figure 7B
SLJ6064	*Matα ndc1Δ::KANMX pURA3-NDC1*	Figure 7B
SLJ6067	*Matα pom152Δ::NATMX ndc1Δ::KANMX pURA3-NDC*	Figure 7B
SLJ001	*Mata NDC1 POM152 LYS2*	Figure 7B

SLJ6968	*Mata sec66Δ::KANMX*	Figure S1
SLJ6997	*Matα sec66Δ::KANMX*	Figure S1
SLJ5102	*Mata kar1Δ::NATMX pURA3-KAR1*	Figure S1
SLJ5099	*Mata mps2Δ::NATMX pURA3-MPS2*	Figure S1
SLJ9338	*Mata bbp1∆::NATMX pURA3-BBP1*	Figure S1
SLJ6059	*Matα ndc1Δ::NATMX pURA3-NDC1*	Figure S1
SLJ4282	*Mata nbp1Δ::HIS3MX pURA3-ADE3-NBP1*	Figure S1
SLJ9449	*Mata sfi1∆::NATMX pURA3-SFI1*	Figure S1
SLJ7686	*Mata sec66Δ::KANMX pURA3-MPS2*	Figure S1
SLJ7687	*Mata mps2Δ::NATMX pURA3-MPS2*	Figure S1
SLJ7688	*Mata sec66Δ::KANMX mps2Δ::NATMX pURA3-MPS2*	Figure S1
SLJ7690	*Matα sec66Δ::KANMX pURA3-KAR1*	Figure S1
SLJ7691	*Matα kar1Δ::NATMX pURA-KAR1*	Figure S1
SLJ7692	*Matα sec66Δ::KANMX kar1Δ::NATMX pURA-KAR1*	Figure S1
SLJ7706	*Matα nbp1Δ::HIS3MX pURA3-ADE3-NBP1*	Figure S1
SLJ7707	*Matα sec66Δ::KANMX pURA3-ADE3-NBP1*	Figure S1
SLJ7708	*Matα nbp1Δ::HIS3MX sec66Δ::KANMX pURA3-ADE3-NBP1*	Figure S1
SLJ7709	*Matα ndc1Δ::NATMX pURA3-NDC1*	Figure S1
SLJ7710	*Matα sec66Δ::KANMX pURA3-NDC1*	Figure S1
SLJ7711	*Matα sec66Δ::KANMX ndc1Δ::NATMX pURA3-NDC1*	Figure S1
SLJ9530	*Matα sfi1∆::NATMX pURA3-SFI1*	Figure S1
SLJ9531	*Matα sec66∆::KANMX pURA3-SFI1*	Figure S1
SLJ9532	*Matα sfi1∆::NATMX sec66∆::KANMX pURA3-SFI1*	Figure S1
SLJ9539	*Matα bbp1∆::NATMX pURA3-BBP1*	Figure S1
SLJ9540	*Matα sec66∆::HYGMX pURA3-BBP1*	Figure S1
SLJ9541	*Matα bbp1∆::NATMX sec66∆::HYGMX pURA3-BBP1*	Figure S1